Master's thesis

Degree Programme in Physical Sciences

Atmospheric Sciences

Derivation of simple proxies for aerosol related parameters at SMEAR III site

Ahmed Hasan Shahriyer

Date: 10/06/2020

Supervisor:

Assistant Professor Pauli Paasonen, Ph.D.

Examiners:

Academician, Professor Markku Kulmala, Ph.D.

Professor Tareq Hussein, Ph.D.

FACULTY OF SCIENCE

UNIVERSITY OF HELSINKI

Helsinki, Finland

HELSINGIN YLIOPISTO
HELSINGFORS UNIVERSITET
UNIVERSITY OF HELSINKI

MATEMAATTIS-LUONNONTIETEELLINEN TIEDEKUNTA
MATEMATISK-NATURVETENSKAPLIGA FAKULTETEN
FACULTY OF SCIENCE

Tiedekunta – Fakultet – Faculty	Koulutusohjelma – Utbildningsprogram – Degree programme	
Opintosuunta – Studieinrikting – Study track		
Tekijä – Författare – Author		
Työn nimi – Arbetets titel – Title		
Työn laji – Arbetets art – Level	Aika – Datum – Month and year	Sivumäärä – Sidoantal – Number of pages
Tiivistelmä – Referat – Abstract		
Avainsanat – Nyckelord – Keywords		
Säilytyspaikka – Förvaringställe – Where deposited		
Muita tietoja – Övriga uppgifter – Additional information		

Abstract:

The local sources influence the spatial distribution of air pollutants in urban settings, and these can be quite diverse. For better air quality forecasting, constant monitoring of pollutants, and a high volume of measurements are necessary at many locations. Building a dense air quality network by only using the reference instruments is expensive and not feasible. The use of complementary sensor like Vaisala AQT 420 can help achieve the goal of creating a robust air quality network. As part of the Helsinki metropolitan Air Quality Testbed (HAQT) project, AQT 420 was tested for its suitability as a complmentary component in an air quality monitoring network. AQT 420 is capable of measuring NO_2, $PM_{2.5}$, PM_{10}, CO, O_3, SO_2, relative humidity (RH), temperature, wind speed (WS), wind direction (WD), and air pressure (AP). Proxies for condensation sink (CS), black carbon (BC), Particle number concentration (N), and Pegasor AQ urban diffusion current ($PAQDC_{LDSA}$, which can be parameterized to calculate lung deposited surface area (LDSA) concentrations) were developed for an urban background site in Helsinki, Finland. The intention is to use variables measured by the AQT 420 and predict additional variables by using proxies. Proxy variables will help to maximize the output of AQT 420 sensors, and giving extra data extraction capability from the sensors. $PM_{2.5}$, NO_2, RH and temperature yielded reliable proxies for both CS and $PAQDC_{LDSA}$ with the correlation coefficient r, 0.85 and 0.83, respectively. While, $PM_{2.5}$, NO_2, and NO_2, RH were enough to produce satisfactory proxy parameters for BC (r, 0.80), and N (r, 0.76), respectively. Additionally, a campaign data for sulfuric acid (SA) from Helsinki, Finland site was used to produce a proxy for SA. SO_2, global radiation, CS and RH gave the best version of that proxy (r, 0.85).

Table of Contents

1. Introduction

Atmospheric aerosols play an important role in moderating climate (Carslaw et al. 2010, Paasonen et al. 2013, Adachi et al. 2010, Mahowald 2011) as well as impacting human well-being (Brook et al. 2004, Oberdörster et al. 2005, Giechaskiel et al. 2009). Aerosols are determined to have a cooling effect on the climate, fractionally mitigating the warming impact caused by the greenhouse gases (Charlson et al. 1992, Makkonen et al. 2012). Increased aerosol concentrations can modify cloud properties resulting in changes to the precipitation possibility (Boucher et al. 2013). Aerosols can alter the amount of light reflected back to space through light scattering (Charlson et al. 1992) or absorption (Flanner et al. 2009). Aerosols containing carbonaceous substances absorb light (Bond et al. 2006). Carbonaceous aerosol depositing on the snow can increase snow surface darkening, which is responsible for springtime warming (Flanner et al. 2009). Additionally, aerosols can also have serious health effects. Aerosols penetrating deep in the lung can cause irritation, inflammation, thus influencing everyday life (Kunzi et al. 2015).

Directly emitted primary aerosol particles contribute to the aerosol number concentrations (Spracklen et al. 2010), along with secondary aerosol particles formed (Kulmala et al. 2004, Metzger et al. 2010, Paasonen et al. 2010, Kulmala et al. 2013) in the atmosphere. The increasing anthropogenic contribution towards aerosol concentrations has become a significant issue. Pollutants emitted from traffic (Rönkkö et al. 2017, Perez et al. 2009), industry, power and heating generation make up a substantial fraction of the anthropogenic emission (Seinfeld and Pandis 2016) in the urban areas. Traffic-related emissions and certain types of urban infrastructures, like street canyons, can create conditions, where people are exposed to pollution for a prolonged period (Pirjola et al. 2012, Rönkkö et al. 2017). As a result, monitoring and forecasting urban air quality and informing citizens beforehand about particular pollution episodes garnered more importance in recent air quality studies (Hussein et al. 2019).

Air pollution components could be trace gases, such as carbon dioxide (CO_2), nitric oxide (NO), nitrogen dioxide (NO_2), sulpher dioxide (SO_2), and aerosol related parameters categorized as particulate matter, such as particle number concentrations (N), black carbon (BC), lung deposited surface area (LDSA), particulate matter mass (PM_{mass}). PM_{mass} dominates the discussions of air quality monitoring and legislation. Still, it is necessary to consider the influence of other particulate matter components. As legislation to curb one element of pollutants may raise a concern to a

different one (Platt et al. 2017). Current particulate mass-based regulation saw the introduction of a filter-based system to diesel engines (Johnson 2008). This system reduced the amount of particulate matter released through the exhaust of a diesel engine. However, a recent study showed gasoline engines are emitting even more particulate matter compared to current filter equipped diesel engines (Platt et al. 2017). The real success of this legislation cannot yet be quantified.

Particles larger than 1 micrometer dominates particle mass size distribution. Nanometer-sized particles, consisting of nucleation, and aitken size range, represents most of the particle number concentrations. Particle size determines the particle residence time in the environment, optical properties, surface area, and health effects (Seinfeld and Pandis 2016). The size and composition of the particles can explain the spectrum of influence exerted by the particles, but details of the health effects are not fully known. In this case, particle area based parameters can be helpful. The surface areas of the particles, in the nuclei, and accumulation size range, are a useful parameter for health effects study (Giechaskiel et al. 2009). The cumulative surface area of smaller particles with a particular mass is much larger compared to the total surface area of larger particles of that same mass (Donaldson et al. 1998). The surface-based chemical impact of particles with the human respiratory system meant more attention is needed to the study of particle size based surface area concentrations (Alföldy et al. 2009).

Combustion products in the fossil fuel burning, wood-burning or forest fires are CO_2, carbon monoxide, water vapour, and soot or carbonaceous matter. Additionally, nitrogen and sulfur oxides, are also produced in the combustion chambers of vehicle engines (Glassman and Yetter 2008), along with some trace metals (Enroth et al. 2016), as a result of addiditves used in engine fuel.

Complete combustion : $fuel + O_2 \rightarrow CO_2 + H_2O$

Incomplete combustion : $fuel + O_2 \rightarrow CO_2 + H_2O + CO + hydrocarbons$

The combustion process produces particles in both gasoline (Karjalainen et al. 2014) and diesel (Rönkkö et al. 2014) engines. There are different processes ongoing in the exhaust plume: new particle formation (Giechaskiel et al. 2005), particle growth through condensation and coagulation (Kittleson et al. 2006). Exhaust plume released from the tail-pipe cools and dilutes rapidly in the ambient condition forming new particles in low temperature and high humidity conditions. The torque that the engine is operating is linked to the particles being of volatile or non-volatile nature (Rönkkö et al. 2006). The engine combustion system also produces Gaseous Sulfuric Acid (GSA).

During high engine torque, GSA is responsible for the formation of nucleation size ranged particles with a volatile core. At low to medium torque, GSA condenses on the particles with a non-volatile (Carbonaceous or metal) core (Rönkkö et al. 2007 ,Rönkkö et al. 2013) and thus responsible for the subsequent particle growth. The presence of accumulation size range particles also determines the formation of particles in engine exhaust. Particles in the accumulation size range act as a sink of the vapours that is responsible for new particle formation, thus preventing the formation of particles that are in nucleation size range (Kittleson et al. 2006).

On-road aerosol size distribution studies showed the presence of nucleation size ranged particles almost all the time. But laboratory studies do not replicate this on all varying conditions (Karjalainen et al. 2016, Kittleson et al. 2006). Ambient conditions probably are more suitable for nucleation to occur (Kittleson et al. 2006). Usually, on the roadside, higher freshly vehicle emitted particles are detected. Dispersion and dilution mechanisms perturb the concentrations, size, and composition of these particles with increasing distance from the road (Pirjola et al. 2006, 2012). The half decay of the particle number concentrations on different urban environments can be different, and depends on the associated meteorological flow dynamics of the individual environment (Enroth et al. 2016). Station for Measuring Ecosystem-Atmosphere Relations (SMEAR) III site situated on a hilltop located at Kumpula, Helsinki Finland is 200m away from a major road (Järvi et al. 2009). Because of the distance, traffic pollutants reach the site after going through dispersion and transformation processes, as meteorological conditions already have a significant effect over that distance (Hussain et al. 2014, Ripamonti et al. 2013).

A dense air quality monitoring network captures the rapidly changeable spatial distributions of the urban air pollutants. Building a dense network based on only the reference level instruments is expensive. As a result, tests are carried out on inexpensive sensors, for their usefulness as a potential component for the air quality monitoring system. Accurate field measurements from the low-cost sensor will give a better resolution for a model in an urban setting compared to a model constructed on just laboratory results (Krecl et al. 2018). As part of the Helsinki metropolitan Air Quality Testbed (HAQT) project, small, inexpensive sensors Vaisala AQT 420 and particle concentration counters are tested. AQT 420 is capable of measuring NO_2, $PM_{2.5}$, PM_{10}, CO, O_3, SO_2, Relative Humidity (RH), Temperature, Wind Speed (WS), Wind Direction (WD), and Air Pressure (AP). At SMEAR III site, aerosol size distributions, black carbon (BC) along with the pollutants and meterological components mentioned above are measured continuously. Further, A campaign running from June 2017-May 2018 was operating a Pegasor AQ Urban instrument at the station.

The parameterized diffusion current of the Pegasor AQ Urban instrument gives the lung deposited surface area (LDSA) concentrations (Kuula et al. 2019). Here un-parametterized diffusion current of Pegasor AQ Urban is levelled as $PAQDC_{LDSA}$ and its proxy was derived.

The relationships among pollutants emitted by traffic exhaust, industrial activity and biomass burning (NO_2, $PM_{2.5}$, BC, N) and further their association with the meteorological conditions were analyzed. Proxies for the aerosol size distribution derived parameters, like paticles number concentration (N), and condensation sink (CS), were developed based on these results. Proxies for BC was calculated similarly. The relevant variables that better predict the BC, N, CS, and $PAQDC_{LDSA}$ were chosen. The resulting optimized parameters using relevant variables will give extra data extraction capability from the AQT 420 sensors. Additional variables will help to maximize the output of these low-cost sensors. Additionally, a campaign running during May 2018 measured Sulfuric Acid (SA) concentrations at the SMEAR III station. This data was used to develop a proxy for SA, while also using the SMEAR III SO_2, global radiation, RH, and temperature data.

2. Background

Aerosol particles are liquid or solid particles suspended in the air or gas medium. Based on the source and formation process, two categories of aerosol particles exist. Those are directly emitted particles and secondary particles formed through the gas to particle conversion and nucleation process. Particles emitted from the combustion, biomass burning, pollen, sea spray, and re-suspension of the dust are a few examples of the direct emissions to the atmosphere. The anthropogenic emissions or emissions that are related to human activity are emission-related to combustion, biomass burning (including wildfires) and industrial activities. Suspension of dust by wind, pollen, and sea spray are examples of direct natural emission of particles.

Once in the atmosphere, the particles can go through various transformation processes, which determines the particle composition and size. In the condensation process, vapors like water or organics condense on smaller particles and changing particle sizes. These same species can evaporate from the surface of larger particles, thus modifying the size of the particles through the evaporation process. The coagulation process, where smaller particles are sticking together to form a more massive particle, occurs all the time. These three processes are examples of the transformation processes that particles go through in the atmosphere.

The chemical composition of the aerosol particles differs according to their sources. Combustion-related primary particles are mainly composed of elemental carbonaceous material and trace metals (Kittleson 1998). The organic carbonaceous element released by the biosphere form a significant fraction of the load of the secondary particles after going through rigorous chemical processes in the atmosphere (Ehn et al. 2014)

Aerosol particles size range varies from nanometer (nm) to hundreds of micrometers (μm) in diameter. Particles, according to their source and their contributing characteristic behavior in the atmosphere, are classified into nucleation (3-30nm), aitken mode (30-100nm) and accumulation size range (100-1000nm) (Seinfeld and Pandis 2016). Traffic-related emission in the urban areas (Rönkkö et al. 2017) and atmospheric secondary particle formation in the boreal forest (Pirjola et al. 1999), marine area (O'Dowd et al. 2002), the free troposphere (Kulmala et al. 2004) contribute significantly towards the nucleation sized particle concentrations. The nucleation sized particles undergo growth processes to larger aitken or accumulation sizes (Paasonen et al. 2018). Some of these particles greater then 50nm can act as cloud condensation nuclei, where water can condense and form cloud droplets and ultimately creating clouds and precipitate.

Fine particles (particles smaller than 2.5 micrometers), and coarse particles (particles larger than 2.5 micrometers) are further two categories of aerosol particles. Additionally, ultrafine particles are particles in the size range of 1-100nm (Seinfeld and Pandis 2016). Fine particles are responsible for the significant portion of the particle mass concentration load in the total atmospheric aerosol mass concentration (Kittleson 1998). $PM_{2.5}$ often denotes the mass concentration of particles below 2.5 micrometers.

The size of the particles determines the lifetime of the particles in the atmosphere. Particles in size range of 0.1-10 micrometers are assumed to have the longest residence time. Dry and wet deposition are two of the foremost important removal processes for these aerosol particles in the atmosphere. Coagulation and diffusion processes remove the smaller particles, and gravitational settling and deposition processes remove the more massive particles rather quickly (Kittleson 1998, Seinfeld and Pandis 2016).

2.1. Sulfuric acid

Sulfur-containing fuel produces sulfur dioxide (SO_2) during combustion processes in vehicle engines, ships and industrial activity. Also, occasional natural contribution coming from volcanic eruptions. While in the atmosphere, SO_2 has a typical lifetime of a week (Seinfeld and Pandis 2016)

and undergo photochemical transformations processes. In ambient condition, hydroxyl (OH) radical is produced through photolysis of ozone (O_3) by photons in the UV-B range (280-320nm, a component in the solar radiation) (Rohrer And Berresheim 2006), and reaction with water molecules. These reactions are summarized as follows.

$$O_3 + h\nu \rightarrow O(^1D) + O_2$$

$$O(^1D) + H_2O \rightarrow 2\,OH$$

SO2 through reactions with oxygen (O_2) and hydroxyl radical (OH) forms sulfur trioxide (SO_3), which in the presence of water can produce sulfuric acid (H_2SO_4) (Stockwell and Calvert 1983).

$$OH + SO_2(+M) \rightarrow HOSO_2(+M)$$

$$HOSO_2 + O_2 \rightarrow HO_2 + SO_3$$

$$SO_3 + H_2O + M \rightarrow H_2SO_4 + M$$

Sulfuric acid (SA) is an essential precursor for the new particle formation in the atmosphere (Weber et al. 1997, Pirjola et al. 1999, Paasonen et al. 2010, Nieminen et al. 2014, Yao et al. 2018). Analysis of the composition of the nucleated particles in the urban setting shows, along with other compounds, sulfur compounds are also present (Kittelson 1998).

2.2. New particle formation in engines

Fuel sulfur content influences the production of GSA in the engine (Arnold et al. 2012). Arnold et al. 2006 further reported measurement of GSA originating from a diesel engine equipped with after Treatment System (ATS). ATS, consists of an oxidation catalyst and diesel-particle filter (DPF), installed in a modern diesel engine helps to remove soot and other metal particles produced in the engine combustion. A small fraction of SO_2 produced in the combustion process oxidize to produce SO_3 at the oxidation catalyst of the ATS. These SO_3 in the presence of water vapor can produce GSA. Lubricant oil may also contain sulfur, and other studies (Rönkkö et al. 2014) mentioned its role in the new particle formation.

Engine after treatment can also determine whether the nucleation is sulfur driven or semi-volatile compound driven (Lähde et al. 2009). At lower air to fuel ratio, higher exhaust temperature coupled with high SO_2 abundance causes GSA concentrations to increase. At increased engine load, higher SO_2 oxidation were observed (Arnold et al. 2012). Gaseous SA emitted from diesel engines

contribute towards the increase of volatile particle concentrations in the nucleation size range at high engine loads. Gaseous SA is formed in the exhaust can also contribute towards the growth of particles composed of non-volatile core (Rönkkö et al. 2013).

The exhaust GSA can go through multiple processes after leaving the exhaust system. GSAs molecules are thought to participate in the formation of nanoparticles (e.g. SA-water, SA – dimethyamine (DMA) - water molecules, SA dimers, and SA- DMA clusters (Yao et al. 2018)) during exhaust dilution (mixing of exhaust plume with ambient air) and cooling (Arnold et al. 2006, Shi et al. 1999). At high dilution ratio and high humidity with lower temperature higher number of nanoparticles are produced, and the size of those particles are around few nm (Yao et al. 2018).

2.3. New particle formation in the atmosphere under ambient conditions

The process of producing newly formed particles from the engine exhaust is a small scale rapid process. Most of the particles are formed rapidly during the dilution and cooling of the exhaust and can influence a small area. On the other hand, new particle formation (NPF) events in the ambient conditions at the atmosphere is an extensive process affecting a vast region. NPF events at several locations in different conditions have been listed in studies (Kulmala et al. 2004). Sulfuric acid-driven NPF events are observed at a boreal forest (Pirjola et al. 1999, Nieminen et al. 2014), remote continental site (Weber et al. 1997), mountain site (Paasonen et al. 2009), and mega-cities (Yao et al. 2018). Also reported are halogen driven NPF events at a coastal boundary layer (O'Dowd et al. 2002) and organic-vapor driven NPF events at a boreal site (Ehn et al. 2014). The volatile organic compounds produced by the biosphere can also go through oxidation processes in the atmosphere. They results in the formation of extremely low volatile organic compounds, and vapors, which can also participate in the NPF events (Ehn et al. 2014). These gaseous compounds go through gas to particle conversions and subsequently produce new particles. Amount of solar radiation, condensation sink, relative humidity, and temperature are important factors that dictate the occurrence of these events (Dada et al. 2017). In a mega-city environment, dimethylamine (DMA) participate as the neutralizing base to stabilize the SA clusters (Yao et al. 2018).

2.4. Number, area and mass concentration derived from the aerosol size distribution

The aerosol particles are spread across a vast size range requiring the aerosol particles to be presented in different statistical means. The characteristics and influence of smaller particles can be quite different compared to the features and impact of larger particles. Thus, based on the characteristics and effects, it is required that the aerosol particles be described in terms of their number, surface area, mass concentrations in a size-based spectrum (Seinfeld and Pandis 2016). Number, area and mass concentrations from the size distributed data from the SMEAR III station are shown in section 4.2. Where also 3 example case studies are discussed to iluminate the influence of arrival of different size distributed aerosol particles at the SMEAR III site.

2.5. Condensation sink

Condensation sink describes the loss rate of condensable vapor onto the surface area of preexisting aerosol particles. These condensable vapors can be responsible for the start of the nucleation process and the growth of particles. Higher condensation sink means a high amount of condensable vapors are lost due to condensation, and is not favorable for the new particles to form. Particles in the accumulation size range contribute most to the condensation sink at a boreal forest site (Lehtinen et al. 2003), while in a coastal site coarse mode particles are important (Dal Maso et al. 2002). Condensation sink is derived from the aerosol size distribution of dry aerosol sizes to get the ambient values (Dal Maso et al. 2005),

$$CS = 2\Pi D \int_0^{D_p} D_p \beta_m(D_p) n(D_p) dD_p = 2\Pi D \sum_{D_{pi}} \beta_m(D_{pi}) D_{pi} N_i \ldots (1)$$

Where,

- D_{pi} is the diameter of the particle size class I, and N_i is the corresponding particle concentrations. This measured size distribution was corrected using the hygroscopic growth factor (Laakso et al. 2004),

  $GF(D_p, RH) = \left(\frac{1-RH}{100}\right)^{\gamma} \ldots (2)$, GF is the growth factor of a particle at a relative humidity RH.

  Where, $\gamma = -3.1116 * 10^5 * D_p - 0.0847 \ldots (3)$ (Hämeri et al. 2001)

- D is the diffusion co-efficient of the condensing vapors.
- The correction factor β_m is calculated from,

$$\beta_m = \frac{1 + K_n}{1 + \left(\frac{4}{3\alpha_m} + 0.337\right) K_n + \frac{4}{3\alpha_m} K_n^2} \ldots (4)$$

where α is the sticking coefficient and K_n is the Knudsen number.

$K_n = \frac{2\lambda}{D_p'} \ldots (5)$, λ is the effective mean free path of the vapor molecules in the gas.

2.6. Black carbon

Traffic, industrial, and residential biomass burning are responsible for the emission of BC particles, which is produced because of incomplete combustion. In the combustion process of carbon-based fuel, BC is produced in the flame and it is then released to the atmosphere as carbon agglomerates. The dry and wet deposition dominates the atmospheric removal process for the BC particles. In the atmosphere, BC particles can go through the aging process, where condensation of soluble material onto BC agglomerate can change the particle composition and carbon fraction of the particle. As a result, the lifetime of these particles and their interactions with the atmosphere can vary considerably. The lifetime of BC particles can be quite short from 2-14 days and influencees both regional and global climate (Bond et al. 2011 Hienola et al. 2013). The position of the soot particles within an aged aerosol particle also determines the climatic interactions and radiative forcing. There is a considerable difference between climate models, which assumes soot particles to be located at the center of the aged aerosol (Bond et al. 2004) compared to the soot particles being in outer positions (Adachi et al.2010).

Climatic effects of BC are the absorption of solar radiation by BC, modifications of the cloud forming processes and deposition of BC on snow. The settling of the BC on snow can change the reflectivity of the snow leading to changes in the albedo of the snow-covered area. Darker snow-covered regions can lead to an increase in radiation absorption, further speeding the heating and melting of the snow (Flanner et al. 2009).

BC particles are generally emitted to the atmosphere with other particles, metals, and trace gasses. These co-emitted pollutants themselves can change the composition of the BC particles along with the organics that are present in the atmosphere. BC particles can act as a core particle, where

volatile and semi-volatile organic can condense. It is observed that the ratio of organics to BC increases with increasing distance from the highway (Enroth et al. 2016). Though BC is not water-soluble, their interaction with the organics means aged BC can become water-soluble. They are thus becoming more suitable for participating in the cloud formation process and change the number concentrations of cloud condensation nuclei.

2.7. Lung deposited surface area (LDSA)

Particles mediated lung injuries are associated with the number of particles penetrating to lung, the shape of the particles and the reactivity of the particles towards the lung cell wall. The health effects caused by the non-fibrous particles are explained using the surface area of the relevant particles. The number concentrations of ultrafine particles are higher compared to the number concentrations of the fine particles of the same mass. The total surface area of the ultrafine particles is more significant compared to the fine particles (Donaldson et al. 1998).

Deposition of a higher number of ultrafine particles on the lung cell wall after inhalation means the clearance of these particles takes longer compared to the fine particles. As a result, ultrafine particles are more likely to travel to Interstitium (a medium of liquid comprising of water and solutes that exists between, for example, the cell wall of skin and to the internal organs) compared to the fine particles of the same mass. Clearance of the particles from the pulmonary tract can happen through a process called phagocytosis. In this process, a type of white blood cell called Macrophages engulfs and digests foreign substances. These foreign substances do not have proteins that are specific to healthy blood cells. A large number of ultrafine particles deposited in the pulmonary tract hampers the ability of phagocytosis - shown in a study conducted on rats (Ferin 1992).

The surface area of non-toxic and non-fibrous particles like carbon and titanium dioxide is an important parameter to describe the toxicity of those particles towards lung cell wall. Because of the longer retention of the ultrafine particles by the lung wall, the surface area of the deposited particles and the surface area of the lung have a longer time to interact. This more extensive interaction may lead to complex surface chemistry to take place. Substances released from the surface of those particles, through surface chemical processes are responsible for moderating the oxidative stress of the epithelial cell surface. Results in the inflammation of the lung walls and transfer of materials from the particles to the surface of epithelial cells and the subsequent interactions with the surface (Donaldson 1998).

The effect of the aerosol mass fraction on the human respiratory tract can also be described based on the biological response of the tract to the volatility of the aerosol. Volatile and non-volatile aerosol mass fractions are responsible for the chemical and physical effect to the human lungs, respectively. Volatile fraction dissolves in the lung fluid, and this interaction with the lung is in chemical nature, thus referred to as chemical effects caused by the particles. On the other hand, non-volatile mass fraction interacts with the lung through the surface of the particles. The surface area of the particle is an essential parameter in this case, and thus, the effect is referred to as physical effects caused by the particles (Giechaskiel et al. 2009).

Alföldy et al. 2009 and Giechaskiel et al. 2009 further demonstrated the physical effects of the non-volatile mass fraction of the particles to be associated with the surface area distribution of the particles in accumulation mode size range. The volatile mass fraction of the particles, responsible for the chemical rasponses, is associated with the volatile mass distribution of the particles in nucleation mode size range, and volatile mass distribution that is condensed over the surface area of particles in the accumulation mode size range, which is described by the accessible surface area distribution of particles in accumulation mode size range.

3. Measurements and methods

3.1. Measurements

The data used in this analysis were measured at Station for Measuring Ecosystem-Atmosphere Relations (SMEAR) III. The site located in Kumpula, 5 km northeast of the center of Helsinki, Finland, lies on a hilltop and measurements are conducted on the ground level as well as on a 31-m high tower. It is an urban background atmospheric constituent measurement facility. The measurement site is surrounded by buildings, parking lot and a small patch of deciduous forest. One of the major road heading to Helsinki is located about 200m southeast of the measurement site. The surroundings of the measurement site can be described according to the surrounding land use and thus classified into three areas of the road (40-180°), vegetation (180-320°) and residential (320 - 40°) section (Järvi et al. 2009). Seasonality in the measured concentrations is observed at the Helsinki sites (Hussain et al. 2004, Pirjola et al. 2006). The observed difference in the concentrations during weekdays and weekends indicates traffic influence in Helsinki (Hussain et al. 2004).

Table 1: Measurement instruments, data coverage and time line of the analysis for the atmospheric constituents and meteorological variables measured at the SMEAR III site.

Atmpspheric constituents and meteorological variables	Instrument	Data coverage	Data Analysed (proxy)				
			N	BC	CS	$PAQDC_{LDSA}$	SA
Air temperature (T)		10/2005 -	11/2010 - 12/2014	02/2018 - 11/2018	02/2018 - 07/2018	02/2018 - 05/2018	05/2018 - 06/2018
Relative Humidity (RH)		01/2001 -					
Wind Speed (WS)		04/2005-					
Wind Direction (WD)		04/2005-					
Global radiation (GlobRad)		10/2001-					05/2018 - 06/2018
Particle number concentrations (N)	Differential Mobility Particle Sizer (DMPS)	05/1997-					
Black Carbon (BC)	Multi-Angle Absorption Photometer (MAAP)	04/2015-		02/2018 - 11/2018	02/2018 - 07/2018	02/2018 - 05/2018	
Particulate matter mass ($PM_{2.5}$)	Tapered Element Oscillating Microbalance (TEOM)	01/2018-					
Particle size distribution data	Differential Mobility Particle Sizer (DMPS)	05/1997-	11/2010 - 12/2014				05/2018 - 06/2018
Nitrogen oxides concentration (NO_x)	Chemiluminescence analyzer	11/2005 -		02/2018 - 11/2018	02/2018 - 07/2018	02/2018 - 05/2018	
Nitrogen oxide concentration (NO)	Chemiluminescence analyzer	11/2005 -					
Sulfur dioxide concentration (SO_2)	UV fluorescence analyzer	09/2006 -					05/2018 - 06/2018

- Pegasor AQ Urban (White 2018) was operating at the SMEAR III site from 06/2017 – 05/2018 and its diffusion current is represented by $PAQDC_{LDSA}$ was. Lung deposited surface area (LDSA) data calculated from the DMPS has a strong correlation with the pegasor AQ Urban instrument's diffusion current (Kuula et al. 2019).
- BC data from traffic sites (Mannerheimintie, Mäkelänkatu, Tikkurila), urban (Kallio) and rural (Luukki) background environment, and small house residential area (Itä-Hakkila) had data coverage from 01/2018 – 12/2018. These measurement sites are operated by Helsinki Region Environmental Services Authority (HSY).

The details about the atmospheric relevant pollutants continuously measured at the site were reported in the Järvi et al. 2009. Several other new instruments (e.g. for $PM_{2.5}$, BC) has since been added to the station for continuous measurements (Petäjä et al. 2018). These continuously measured data of different pollutants and meteorological variables were downloaded from the smart smear website (https://avaa.tdata.fi/web/smart/smear). Table 1 shows the full data coverage for all the variables.

Particle number concentration (N) is derived from the particles size distribution data measured by the Differential Mobility Particle Sizer (DMPS; Aalto et al. 2001). Condensation sink was also derived from the size distributed particles data using the method described by Dal Maso et al. 2002. Particle number concentration, and condensation sink data from 2010-2014, and (February – July) 2018, respectively were analysed. Particulate matter ($PM_{2.5}$) measured with Tapered Element Oscillating Microbalance (TEOM) was used to construct black carbon (BC) proxy for the SMEAR III Kumpula site. Multi-Angle Absorption Photometer (MAAP) is continuously measuring black carbon concentrations from January 2018. Working principle for the TEOM (Mayer et al. 2000) and MAAP (Petzold et al. 2005) are described in the referenced literature.

Further, $PM_{2.5}$, NO_2 and BC data provided by the HSY (Helsingin seudun ymparistopalvelut-kuntayhtyma) for several other locations were later used to investigate the performance of the Kumpula BC proxy by comparing measured BC concentration with proxy concentration for those other locations. TEOM was also used in the other HSY sites for measuring $PM_{2.5}$.

Trace gas nitrogen dioxide (NO_2) concentration is derived from the continuously measured nitrogen oxides (NO_x) and nitrogen oxide (NO) concentrations. NO_2 concentration data was used as a component to construct several proxies (Particle number concentration, Black carbon, Condensation sink). Another continuously measured trace gas, sulfur dioxide (SO_2) was used to calculate the sulphuric acid proxy.

Sulfuric acid is measured with the Chemical Ionization Atmospheric Pressure Interface Time-of-Flight Mass Spectrometer (CI-API-TOF) instrument at the SMEAR III site, and data coverage for the sulfuric acid was May - June 2018. Working principle and calibration of the CI-API-TOF instrument has been described in the referenced literature (Junninen et al. 2010).

Additionally, meteorological data such as Relative Humidity (RH) and temperature, along with global radiation, were used for the construction of several proxies.

3.2. Proxy calculations

Measurements of atmospheric constituents are conducted all the time. Some of those are continuous measurements while others cover a smaller time-period (e.g. one month), usually in a measurement campaign. Complications, expenses, remote locations and feasibility often dictate whether a measurement is conducted continuously or in short campaigns. Data gathered from shorter campaigns can be mathematically derived to represent it over an extended period (e.g. one year). These calculations often use variables that show some relation or association with those hard to measure constituents. A function representing one variable, derived from other related variables, is called a proxy.

In general, for all respective 1st level proxy calculation in this analysis, y-axis data contains variables for which the proxy is being derived, and the x-axis contains the prospective variables that are going to used to build the proxy equation. Linear least square method was followed for the derivation of the fitted function. Often for the initial 1st level proxy, both data-set for x and y-axis were converted to logarithmic values, but the choice of log or linear scale depends on the assumed dependence between the main variable and the prospective proxy variable. The fitted line for the logarithmic values has the form,

$$\log Y = a_1 \log X_1 + \log b_1 \ldots (6)$$

Where, a and log b are the slope and intercept in the log-log plot, and log X and log Y are the logarithmic values of X and Y variable.

The converted linear equation is,

$$Y_{1st} = f(X_1) = b_1 * X_1^{a_1} \ldots (7)$$

Here, the measured variable, Y_{mea} is approximated using the variable X_1 and the fitted parameter.

For 2nd or higher level proxy, the prospective proxy variables used were sometimes in the linear (e.g. RH and Temperature) or logarithmic (e.g. NO_2, $PM_{2.5}$) scale. Both linear and logarithmic scale was tested for these variables where it was possible, and one showing the better association was used for the proxy calculation.

For the calculation of 2nd level proxy, the ratio of measured concentration to the 1st level proxy concentration was taken, and logarithmic values of the ratios were plotted on the y-axis. The new

variable that is to be used in the x-axis was either in the linear (semi-log plot) or logarithmic (log-log plot) form. In the case of the semi-log plot the fitted line is represented as,

$$\log\left(\frac{Y_{mea}}{Y_{1st}}\right)=a_2*X_2+\log b_2 \ldots(8)$$

which after rearranging and in linear scale is,,

$$Y_{2nd}=\left(b_2*10^{a_2*X_2}\right)*Y_{1st} \ldots(9)$$

replacing $Y_{!st}$ from the previous equation,

$$Y_{2nd}=b_1*X_1^{a_1}*b_2*10^{a_2*X_2} \ldots(10)$$

Or, in the case of log-log plot the fitted line is represented by,

$$\log\left(\frac{Y_{mea}}{Y_{1st}}\right)=a_2*logx_2+\log b_2 \ldots(11)$$

After rearranging and replacing the value for Y_{1st} the equation becomes,

$$Y_{2nd}=b_1*X_1^{a_1}*b_2*X_2^{a_2} \ldots(12)$$

This procedure was followed for adding more variables to the proxy equation until the final level of proxy can not be made any better with the addition of more variables. This similar approach was followed to approximate the concentrations of monoterpenes and their oxidation products for SMEAR II site at Hyytiälä, Finland (Kontkanen et al. 2016). The final level of proxy was further optimized by the method described by Paasonen et al. 2009, Where the ratio of measured to the final proxy was taken and then the slopes and intercepts that reduce the ratio of 90th percentile to the 10th percentile were calculated using the MATLAB function fminsearchbnd. The final optimized equation can be expressed as,

$Y_{final}=Constant*X_1^{a_1}*X_2^{a_2}\ldots,\ldots(13)$, in the case where all of the variables were in logarithmic scale when fitted parameters were calculated, and then converted to linear equation.

$Y_{final}=Constant*X_1^{a_1}*10^{a_2*X_2}*X_3^{a_3}\ldots,\ldots(14)$, in the case where variables are a mixture of linear and logarithmic form when fitted parameters were calculated, and then converted to the linear form.

3.3. Uncertainty calculation

The performance of the optimized proxy was evaluated using the uncertainty calculation method described by Mikkonen et al. 2011, where the equation calculates the uncertainty related to the proxy when compared to the measured value,

$$Uncertainity = \left(n^{-1} \sum_{i=1}^{n} \left| y_i - \hat{y}_i \right| \right) * \bar{y}^{-1} \ldots (15)$$

where n is the number of observations, y_i is the measured concentrations, $\hat{y}$ is the optimized proxy concentrations, and $\bar{y}$ is the mean of the measured values. The lower the calculated uncertainty value, the better the proxy against the measured levels.

4. Results

4.1. Sulfuric acid proxy

SA was measured during May - June 2018 on a month-long campaign at SMEAR III site,. SA proxy was derived using 30 min average data of SA, meteorological variables, and trace gases. As mentioned in the background information above (section 2.1), SO_2 and global radiation with their photo-chemical association are considered as the source terms for SA in the construction of SA proxy. Figure 1(a) shows the relation between measured SO_2 and SA from ambient conditions, and it shows the expected (Petäjä et al. 2009) positive correlation (r = 0.64). The fitted line gave the first term of the proxy. The function derived from the fitted line was converted to a linear scale as a logarithmic scale was used for measured SO_2 and SA for initial illustration.

The ratio of measured SA and proxy SA strongly correlate (0.65) with global radiation (figure 1(b)). Here, both ratio and global radiation are depicted on the logarithmic scale. Hydroxyl radical (OH) is essential for the SO_2 oxidation in the atmosphere, and the measurement of OH is even more difficult compared to SA. Still, OH has been found to correlate strongly with global radiation (Petäjä et al. 2009, Mikkonen et al. 2011, reference therein). Thus, global radiation is an ideal substitute variable to be included in the proxy.

Condensation of SA on the pre-existing aerosol particles is considered to be one of the vital mechanism through which ambient SA is being lost in the atmosphere. The contribution of pre-existing particles in the condensation process and derivation of the term condensation sink (CS)

from the DMPS aerosol size distribution data is described in section 2.5. The ratio of measured to proxy against the CS in figure 1(c) shows a moderate anti-correlation. At higher CS values, lower SA is expected as those (SA) are lost on the pre-existing particles. Role of CS in a proxy constructed from a combined dataset is found to be minor (Mikkonen et al. 2011).

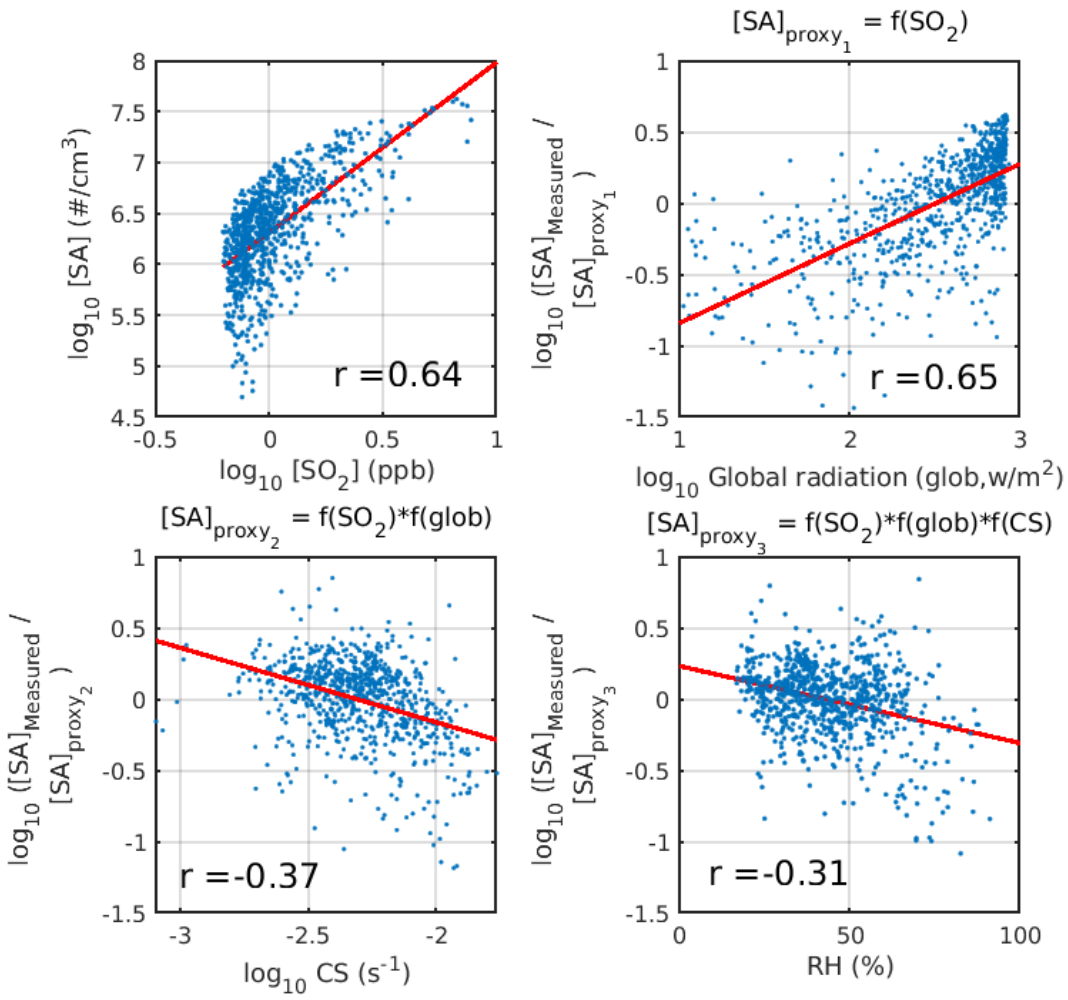

Figure 1: $SA_{proxy,1}$ gives 1st level proxy as a function of SO_2 (1 a), the ratio of $SA_{measured}$ to $SA_{proxy,1}$ as a function of Global radaition (1 b), the ratio of $SA_{measured}$ to $SA_{proxy,2}$ as a function of condensation sink (CS) (1 c) and the ratio of $SA_{measured}$ to $SA_{proxy,3}$ as a function of relative humidity (RH) (1 d) shows the individual steps for the proxy construction. $SA_{proxy,1}$, $SA_{proxy,2}$, and $SA_{proxy,3}$ functions are shown in details in the title of b, c and d subplots of figure 1. Parameters relevant for the fitted functions are presented in the table 2..

RH defined as a sink term from the perspective is that the photochemical production of SA could be inhibited because of lack of radiation during high RH scenarios (Hamed et al. 2011), which could be related to the cloudy environment (Dada at al. 2017). At the same time the SA is being lost

through condensation or coagulation proceses. CS and RH are related to aerosol particles through the hygroscopic growth of particles. Hygroscopic growth is driven by different meteorological and environmental condition. It is often changeable among different sites. Probability of molecules sticking to existing particles increases at high RH condition and thus creating conditions for the growth of particles by condensation of water molecules, SA vapors or oxidized organic vapors, a process that increases the CS. After inncluding CS and RH in the proxy derivation the final proxy equation can be written as,

$$SA_{proxy} = Constant * SO_2^{s1} * Glob^{s2} * CS^{s3} * 10^{RH*s4}. \ldots\ldots\ldots (16)$$

The initial parameters and constant were further optimized according to the method described by Paasonen et al. 2010, and optimized parameters (s1,s2,s3, and s4 and constant) are given in table 2. $V_{90/10}$ is the ratio of 90^{th} percentile to the 10^{th} percentiles of the ratio of measured to proxy concentrations. Purpose of the optimization is to reduce the value of initial $V_{90/10}$. Final $V_{90/10}$ after optimization are reported in table 2. The lower $V_{90/10}$ after optimization suggests the optimization process was successful in making the proxy better with improved final parameters and constant. The uncertainty values reported in table 2 tells the uncertainty associated with the use of a certain proxy. Lower uncertainty values mean the proxy is performing better. There is slightly lower uncertainty related to the use of CS calculated from DMPS compared to the CS predicted from the CS proxy (derived later in section 4.4, which is a function of $PM_{2.5}$, NO_2, RH and temperature). Which is understandable as CS proxy itself has its uncertainty when compared to the derived CS values from the DMPS aerosol size distribution measurement.

Table 2: Final proxy parameters after optimization. The reduction in v values of the ratio of 90^{th} to 10^{th} percentiles mean the proxy has improved after applying optimization method.

Proxy	constant	Slope (s1)	Slope (s2)	Slope (s3)	Slope (s4)	$V_{90/10}$ (unoptimized)	$V_{90/10}$ (optimized)	uncertainty	r
SA (SO_2, Glob, CS, RH)	1.27e4	1.39	0.67	-0.30	-0.0029	3.77	3.52	0.35	0.85
SA (SO_2, Glob, Cs_{proxy}, RH)	2.53e+04	1.50	0.62	-0.22	-0.0029	4.076	3.76	0.39	0.86

Calculating SA proxy with different CS (proxy and measured) also gave the perspective usefulness of using a proxy in calculating a different proxy, and their performance against a measured quantity. The two different SA proxy derived from $CS_{calculated}$ and CS_{proxy} were plotted against the measured SA shown in figure 2. Both SA proxies are performing well, and either one can be used for SMEAR III

site. The correlation coefficient of 0.85 (r, figure 2, table 2) is quite similar to that of a proxy constructed using a combined dataset from various location (r = 0.87, Mikkonen et al. 2011), urban Beijing (r = 0.83-0.86, Lu et al. 2019) or at a boreal forest site (0.81 – 0.90, Petäjä et al. 2009). Varying meteorological and environmental conditions, air mass arriving at the site and seasonality determines the performance of proxy.

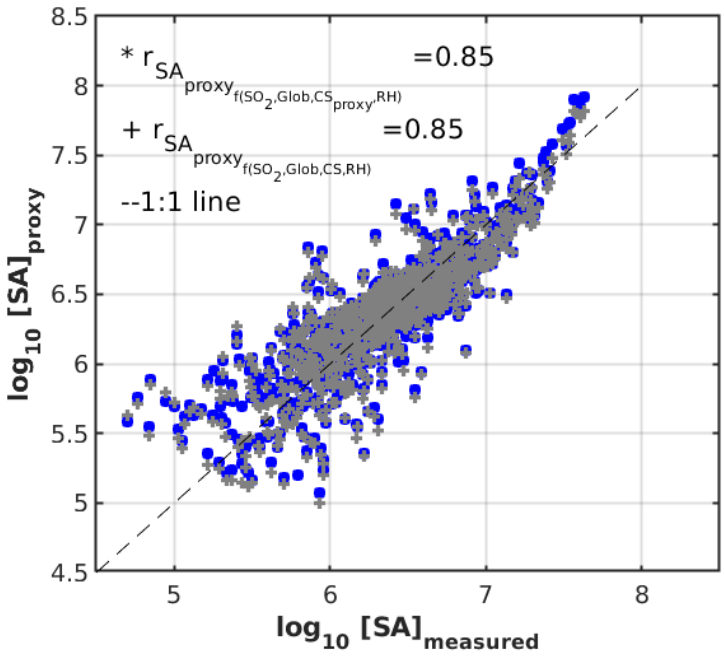

Figure 2: Final optimized SA proxy against measured SA concentration shows the use of condensation sink calculated from the DMPS size distribution data and condensation sink calculated as a proxy from $PM_{2.5}$, NO_2, RH and temperature produces similar SA proxy concentrations.

Diurnal patterns of SA concentration and the variables used in the proxy (Fig. 3) show the gradual increase of the SA concentration as the solar radiation also starts to increase. The maximum SA concentration also coincides with the highest radiation value, depicting the dependence of the production of the SA on solar radiation. The anthropologically emitted SO_2 levels start to increase during morning rush hours with the highest observed values during noon — thus confirming also SO_2's anthropogenic origin for the SMEAR III site. Both CS and RH are at their lowest level when SA is at the highest — thus creating the ideal condition for SA production when SA loss is at a minimum. The daily cycle of SA proxy constructed as a function of SO_2, Global Radiation, $CS_{calculated}$ and RH follows the measured SA nicely except around noon when the proxy is predicting lower concentrations.

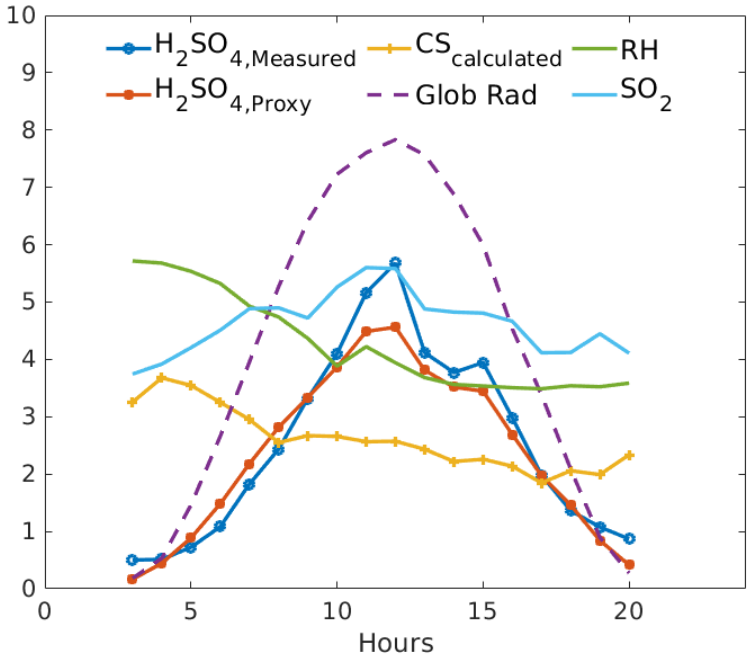

Figure 3: Median diurnal patterns of the variables considered for the SA proxy calculation along with measured and proxy SA concentrations constructed from the hourly median data. Only data where the global radiation was greater then 10 Wm^{-2} was taken. Data coverage was from May 3rd to June 3rd.

Table 3 shows the SA concentration comparisons among measured, proxy calculated from this analysis, statistical proxy equation from Mikkonen et al. 2011 and proxy equation utilising global radiation from Petäjä et al. 2009. Analysing the 50th percentile of the SA concentrations, it was found that $SA_{measured}$ ($2.35*10^6$) and SA_{proxy} ($2.57*10^6$) calculated from this analysis is closest to each other. SA proxy equation of Petäjä et al. 2009 was derived for a rural boreal forest SMEAR II site at Hyytiälä, Finland. At this location, there is very little anthropogenic activity going on. SA concentrations are one order of magnitude smaller in the SMEAR II site compared to more urban SMEAR III site. Using the SMEAR III data, Petäjä et al. 2009 proxy is predicting one order of magnitude lower concentrations compared to measured concentrations for SMEAR III site. Different environmental conditions and different surroundings may explain the differences. The statistical proxy of Mikkonen et al. 2011 can be used for SMEAR III site. As it was prepared by

combining data-set from different environments and theoretically it should perform well for the SMEAR III site. But comparing the 25th, 50th and 75th percentiles, it appears Mikkonen et al. 2011 proxy is predicting a factor of 2 higher compared to the measured SA. The higher predicted values by the Mikkonen et al. 2011 proxy could be related to the proxy being developed using data from more polluted sites compared to SMEAR III site. Based on the above observations, the proxy of this analysis is performing similarly to the measured values compared to the other proxies.

Table 3: Minimum, maximum, 25th ,50th and 75th percentiles of the measured SA and relevant variables for SA proxy.

	RH (%)	Temperature (degree C)	SO2 (PPb)	CS (s^{-1})	Radiation (Wm^{-2})	Measured H_2SO_4 ($\#cm^{-3}$)	Proxy H_2SO_4 ($\#cm^{-3}$)	Mikkonen et al. 2011 ($\#cm^{-3}$)	Petäjä et al. 2009 (($\#cm^{-3}$))
Minimum	16.83	5.78	0.62	0.0008	10.56	$5.04*10^4$	$9.94*10^4$	$8.47*10^6$	$1.79*10^3$
25th percentile	32.47	13.88	0.77	0.0037	199.85	$1.09*10^6$	$1.30*10^6$	$1.84*10^6$	$8.17*10^4$
50th percentile	42.23	17.68	0.92	0.0050	450.90	$2.35*10^6$	$2.57*10^6$	$4.52*10^6$	$2.06*10^5$
75th percentile	54.10	20.76	1.20	0.0068	687.83	$4.50*10^6$	$3.89*10^6$	$7.07*10^6$	$3.58*10^5$
Maximum	91.07	29.12	7.70	0.0172	857.56	$4.27*10^7$	$6.63*10^7$	$2.76*10^7$	$2.97*10^6$

4.2. Charecteristic description of aerosol size distribution at SMEAR III

Figure 4 shows particles from the nucleation (3-30nm), aitken (30-100) and accumulation (100-1000) size range (Seinfeld and Pandis 2016) contributing to the Particle number concentration at the SMEAR III site. The maximum contribution to Particle number concentration is coming from particles in the aitken size range. The peak concentration of particles is around 40 nm, which falls near the smaller aitken sizes. Laboratory and ambient condition measurements showed engines produce bimodular distributions in the number size distributions spectra (Kittleson et al. 2006 a,b). Right next to the road vehicle exhaust contributes maximum towards the particles in the nucleation size range (Kittleson et al. 2006a). Also, engine fuel loads and driving conditions influence the particle sizes.

Particle number concentration always vary with different environmental conditions (Kittleson et al. 2006a). Maximum Particle number concentration is expected to be near the roadside, while further away from roadside dispersion processes means the levels can reduce significantly (Pirjola et al. 2006). Also, traffic alone can not explain the annual cycle of Particle number concentration, as there are other sources important for the smear III site. The particles arriving at the SMEAR III site are considerably aged and gone through dispersion and transformation process. Our measurement site is

200m away from the roadside, on a hilltop, and particle measurement is conducted at 4m height. So Particle number concentration can vary from the readings performed right next to the road. Previous investigations on the contribution by the local sources on the measured pollutants yielded a wide spectrum of influences that is categorized to local traffic, residential, vegetation, secondary formed particles, and the effect of long-range transport and local meteorological conditions (Ripamonti et al. 2013).

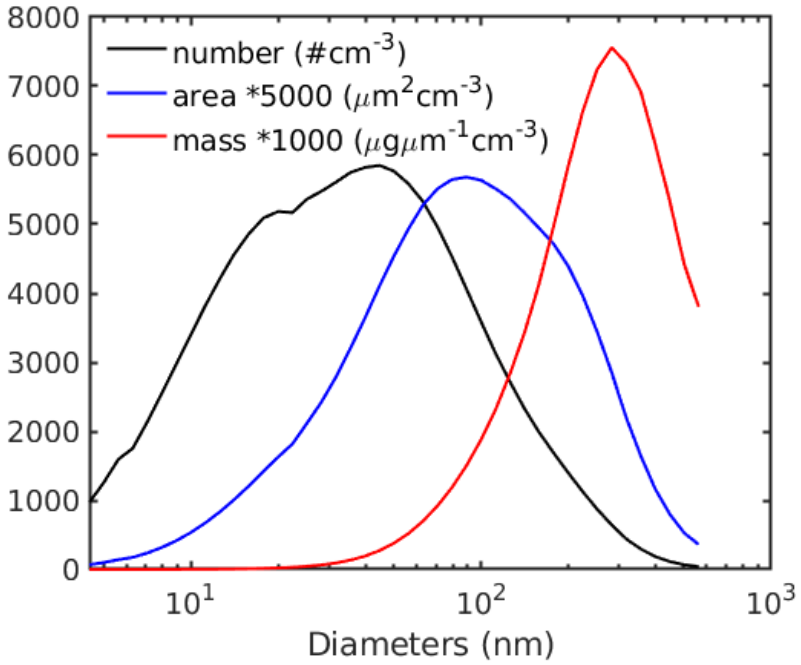

Figure 4: Aerosol number (black line) , surface area (blue line) and mass (red line) size distribution from DMPS data for 2010-2014. Area and mass size distributed concentrations were scaled by the factors mentioned on the top left of the figure to fit all three size distributions in the same figure.

Particles in the nucleation aitken, and accumulation size range make up most of the Particle number concentration spectrum. Nucleation size range particles are formed during the exhaust dilution and cooling process and are assumed to mainly consists of sulfur compounds and hydrocarbons (Kittleson et al. 2006a). At this site, local traffic emission dominates the 20-40 nm size range with high particles concentration when the wind was blowing from the road section (Ripamonti et al. 2013). Further, traffic contributed to the smaller particle sizes during cold winter months. High particles concentration get enhanced because of the lower mixing in the boundary layer (Järvi et al. 2009).

Particles in the accumulation size range make up almost all of the masses of the aerosol particles and thus dominates the aerosol mass-size distribution (Seinfeld and Pandis 2016) (also, figure 4, mass concentrations). The surface area concentrations at the SMEAR III station is mainly dominated by the particles from larger aitken and accumulation sizes (Figure 4, Surface area concentrations).

Examples of aerosol size distributions during winter (figure 5), early spring (figure 6) and late spring (figure 7) have been described below. By no means, this gives the full picture for the SMEAR III site, as this was not the goal of this work. This section was added to this analysis to give a glimpse to the different conditions and sources that could be driving the detection of aerosol particles and size distributions.

4.2.1: Cold winter days

Two cold winter days (Feb 5th and 6th) are depicted in figure 5, where the top panel shows the aerosol size distributions and associated Particle number concentration (N). The first investigated day is a clear, sunny day (see global radiation on 3rd panel, figure 5), and the traffic influence can be seen from the increase in the NO_x (panel 5) and N (panel 4) concentrations around rush hour. The newly formed particles from 6 am until 6 pm is probably related to the particle formed during the engine plume dilution and cooling processes. This day is also characterized by the relatively high humidity (68-82%, panel 6) and low condensation sink (panel 3). On this day wind speed was variable (1-13 ms^{-1}) and most of the time stayed in the higher percentile of that range, and wind direction remained constant around 100^{o}, a direction to the road section (these are not shown here).

Feb 6th is not a clear day (according to the global radiation on panel 3), and there are high number of particles from 6 am to noon. Wind speed was low (1-3 ms^{-1}) and wind direction remained similar to the previous day, perhaps moved to a more eastern direction (90^{o}) (not shown here). Low wind speed could affect the dispersion of particles. N remained somewhat constant or slightly lowering later in the day and not as variable as the day before. Higher condensation sink is also seen on Feb 6th from the day before and continued to increase later in the day.

There is new particle formation gooing on in the exhaust system itself along with the particle formed during the plume dilution and cooling process. These nucleated particles ages and more organic materials get condensed on the surface of these particles. This process helps them to grow into larger sizes and could results in changes to the characteristics of the particles compared to the original exhaust emitted particles. Carbonaceous particles emitted from vehicle exhaust are often

hydrophobic. Their transformation in the ambient conditions means that they turn hydrophilic after some time and water vapour can condense on them. Growth to larger particles in the accumulation size range means they can act as cloud condensation nuclei.

Volatile nucleation mode sized particles coagulate with accumulation mode sized particles and are not detected during measurements. Nonvolatile fractions and carbon agglomerates are also constituents of the directly emitted accumulation mode particles. (Kittleson et al. 2006a). Figure 5 could be an example of new particle formation due to traffic and detail analysis over many days are needed for a better conclusion.

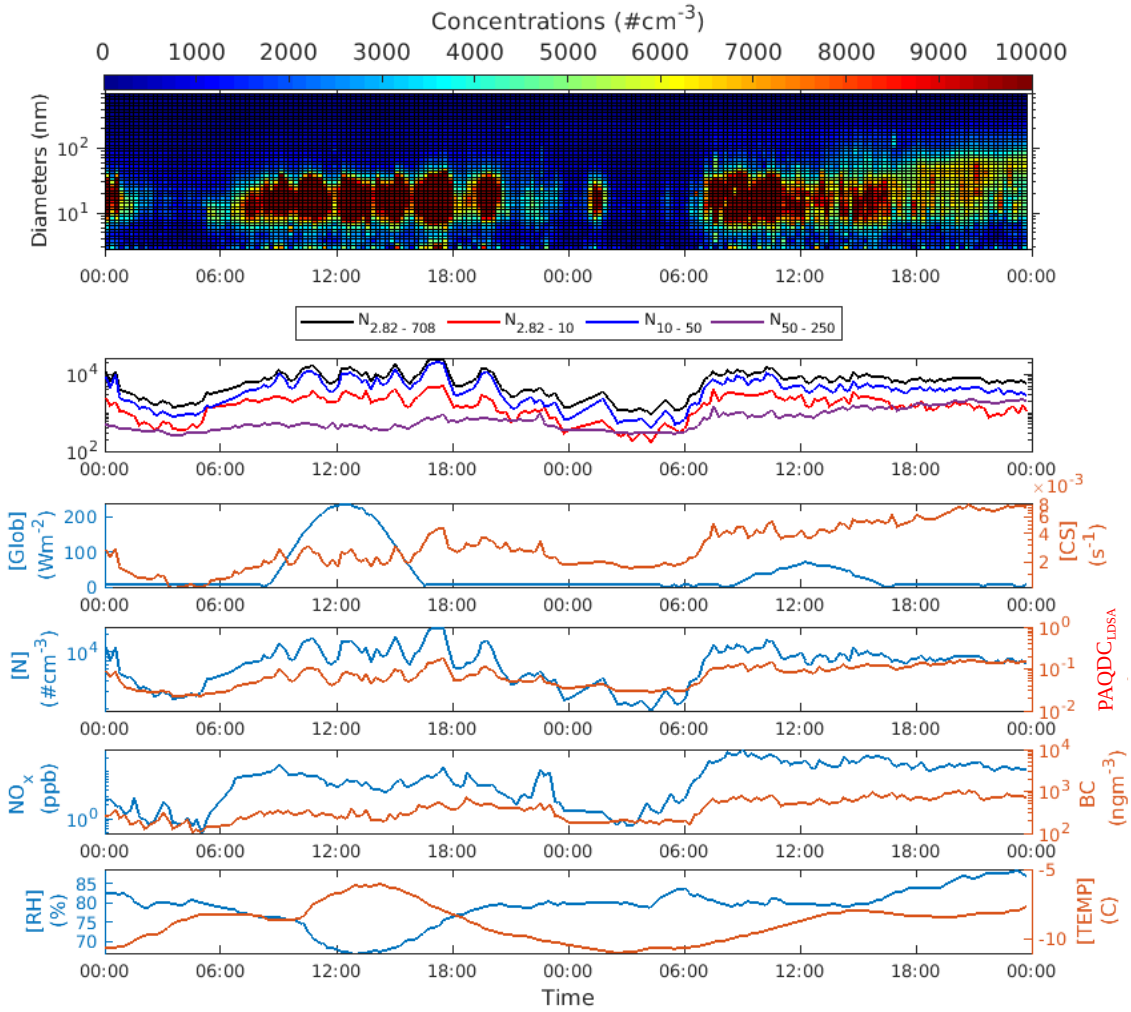

Figure 5: Aerosol size distributions over February 5th and 6th along with time series plots for various atmospheric pollutants and meteorological parameters. Suspected new particle formation in the exhaust and exhaust plume dilution process can be seen on February 5th. Which is not that pronounced during February 6th.

4.2.2: New particle formation events in early spring

A significant number of NPF events occurs during the daytime, at end of winter beginning of spring (Nieminen et al. 2014). New particle formation in the ambient conditions was observed on early spring on both March 26th and 27th (figure 6). March 26th is a clear day (global radiation, panel 3), condensation sink (panel 3, right y-axis) was low before the start of the event, RH is low enough, and the temperature is also in the suitable range for particle formation (Dada et al. 2017). The start time of this event is around noon. The event and growth of particles were quite pronounced. These newly formed particles grow to larger sizes, and this is visible for the rest of the day. The non-detection of the continuous growth process next day coincide with the morning rush hour (March 27th), and also with the change in wind direction (not shown here). So the air mass that was responsible for NPF event and particles growth were not visible anymore at the SMEAR III site.

After a brief change in the wind direction during rush hour, the wind direction returns to the previous day's direction. Again a new particle formation event on March 27th started around afternoon, and somewhat similar growth in particles is observed like previous day . Non-detection of the growth process next day (March 28th) again coincides with the morning rush hours but this time no significant change in the wind direction was observed. Wind speed for all the days shown in the figure remained between 2-6 ms^{-2}. On March 27th, the condensation sink is lowest around the start of the event, the day was intermittently cloudy (global radiation, panel 3, figure 6). Further, for both days, the growth of particles to larger sizes, and an increase in concentrations of more massive particles accompanies the rise in $PAQDC_{LDSA}$ concentrations.

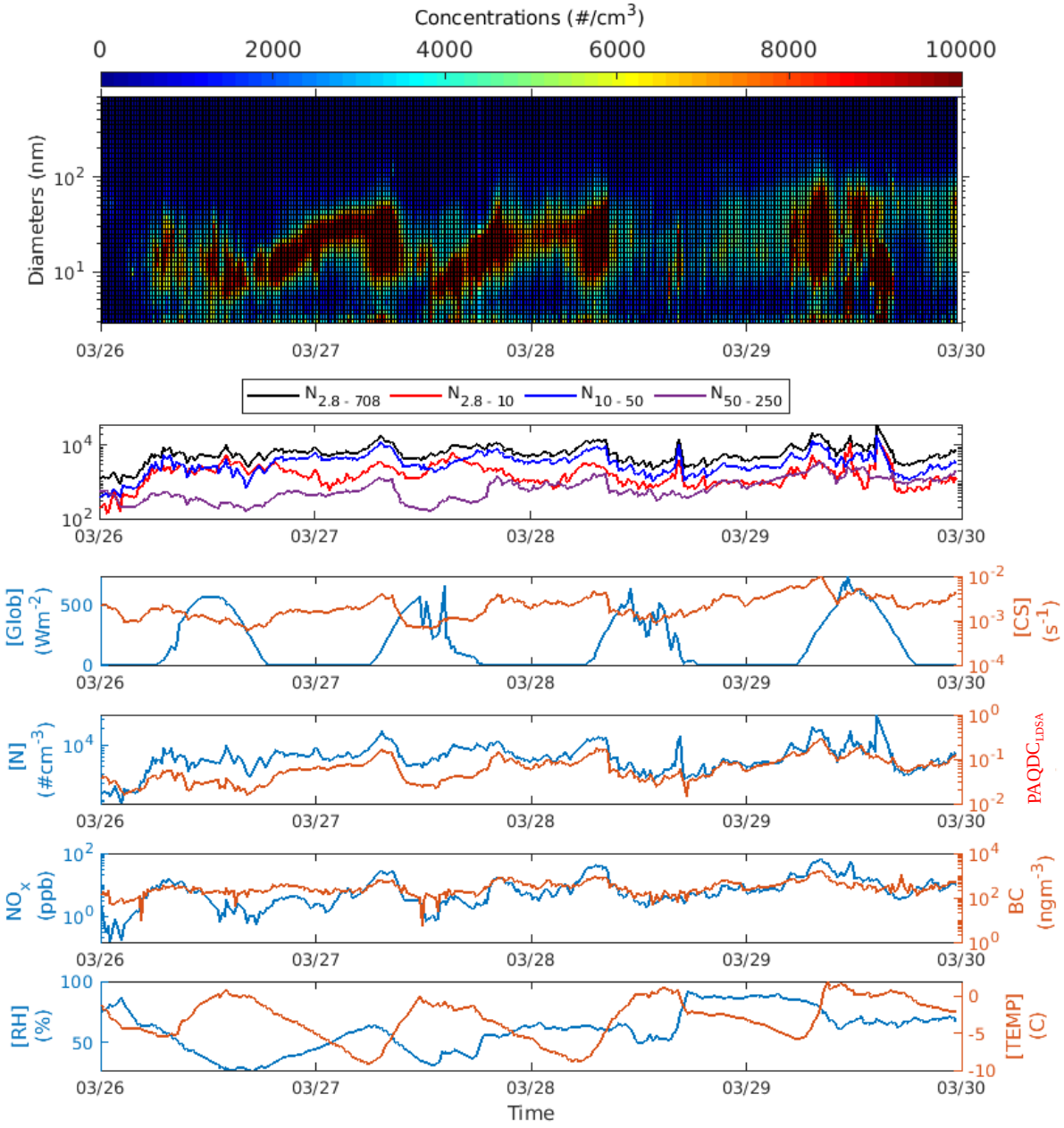

Figure 6: NPF events at ambient condition during March 2018 at Smear III site. The associated times series of the atmospheric pollutants and meteorological parameters.

4.2.3: Long range transport episodes in late spring

At the SMEAR III site, long-distance sources are thought to contribute towards the larger accumulation sized particles during warm periods (Ripamonti et al. 2013). Particles in the accumulation size range prevent the appearance of particles in nucleation size range. As the smaller particles coagulate with larger particles, results in the absence of the particles in the nucleation size range during the warm period (Hussain et al. 2014).

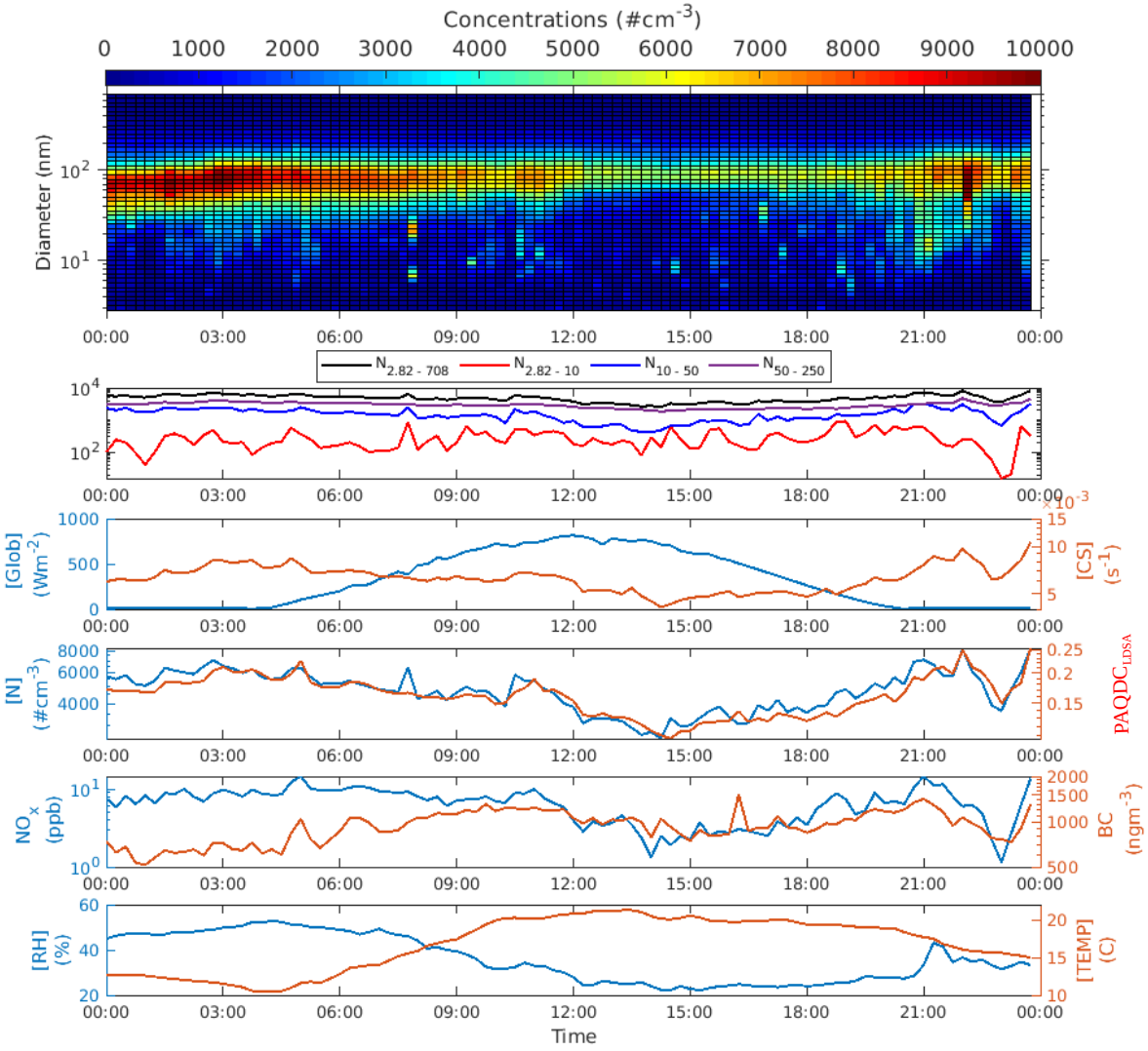

Figure 7: Long-range transport episode at SMEAR III site on May 12th 2018, similar conditions are regularly observed during the summer, not shown here. One example day is presented here. The accompanying time series are of atmospheric pollutants and meteorological parameters.

An example of long-range transport episode at the SMEAR III site is depicted in figure 7. The inter-connectivity between particle concentrations and $PAQDC_{LDSA}$ (panel 4) and particle concentrations with CS (Panel 3,4) is also visible..

Overall, Figure 4, 5, 6, and 7 shows the connectivity between the various aerosol size distribution derived concentrations, and various atmospheric pollutants and meteorological conditions. These example analysis indicate the significant contribution of different types of sources and processes at SMEAR III site. The underlying factors governing particle population in ambient conditions around SMEAR III site or Helsinki, in general, are wide-ranging.. More detailed analysis will be needed to create a complete picture, but this was not the goal of this work.

4.3. Particle number concentration proxy

The presence of NO_2 in the exhaust plume has long been reported (Magnus Lenner 1987, Kurtenbach et al. 2012). At low engine speed, NO can stay longer in the exhaust system. In the presence of excess O_2, NO can get oxidized to produce NO_2, which is then emitted to the ambient air by the exhaust system. Particle concentration and NO_2 concentration correlate ($r = 0.71$) well over the long period (2010 - 2014) of analyzed data (figure 8). Maximum correlation between particle number concentrations and NO_2 is observed during winter (Järvi et al. 2009). This can indicate the traffic influence on the emission of both particles and NO_2. Traffic impact is less visible during spring and summer months when new particle formation is an additional significant contributor towards the particle numbers. Comparative analysis of the weekdays and weekends also confirms the traffic influence at the site (Hussain et al. 2008).

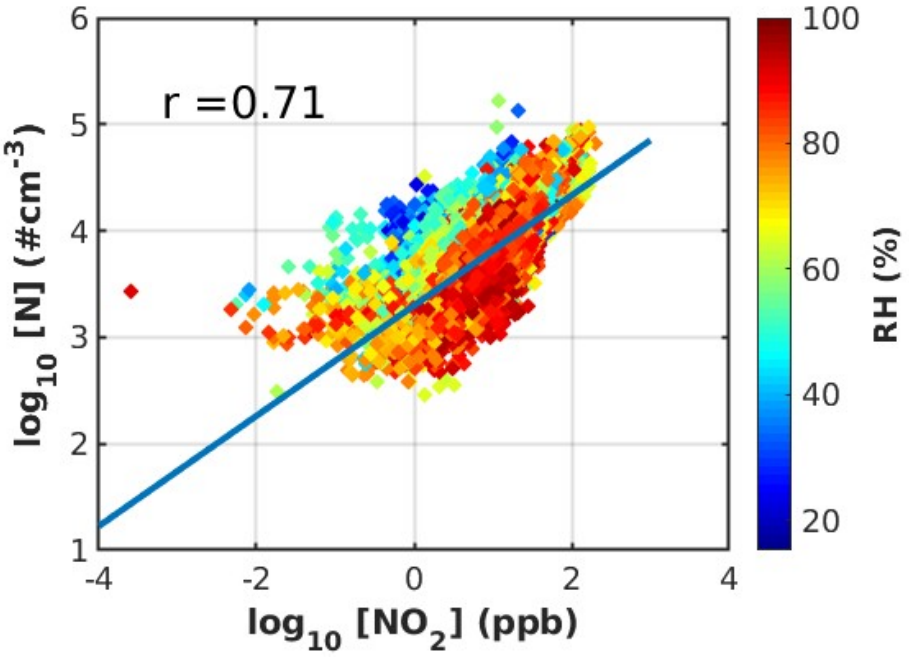

Figure 8: Particle number concentration (N) as a function of nitrogen dioxide (NO_2) with corresponding relative humidity (RH) shown by the colorbar. Correlation between N and NO_2 is given by the correlation coefficient r. The blue fitted line corresponds to the fitted function. Resulting fitted parameters are reported in table 4. All data points are half an hour average points for the time-period of Nov 19th 2010 – Dec 31st 2014.

NO_2 probably does not contribute towards particles composition, as studies (Kittleson 1998, Kittleson et al. 2006, Enroth et al. 2016, Rönkkö et al. 2013) often mentioned other compounds or materials, but no precise NO_2 based compounds. Both particles and NO_2 are produced during the exhaust combustion, and exhaust dilution and oxidation processes. They are co-emitted in the exhaust gas. While NO_2 may not make up the composition of exhaust emitted particles, but as a co-emitter from the exhaust system, NO_2 can be used as an indicator for traffic emissions. NO_2 can be used as the first component of Particle number concentration proxy to predict the ambient particles levels.

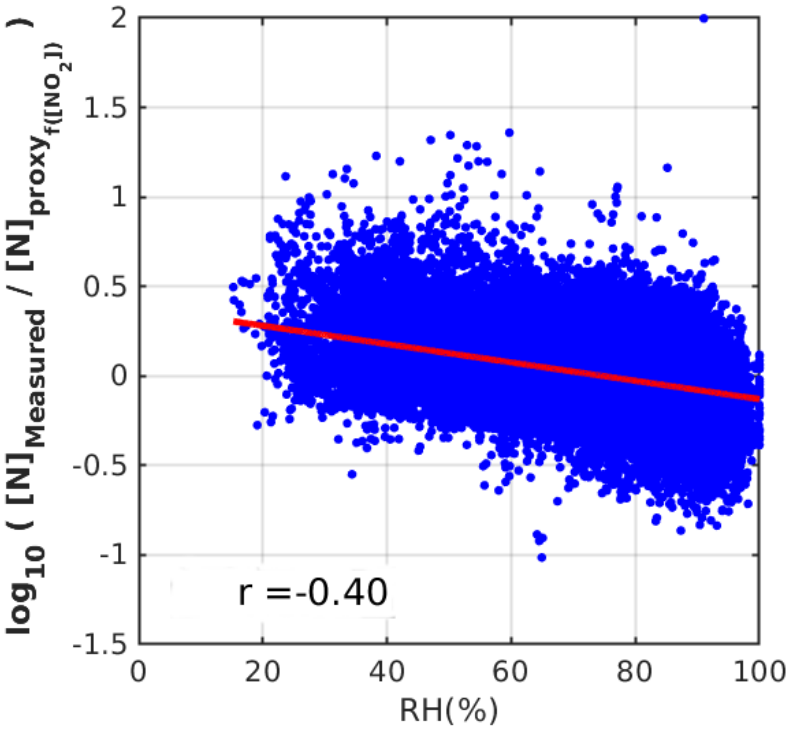

Figure 9: The ratio of observed N to the predicted N plotted as a function of RH shows moderate anti-correlation. Red fitted line is the fitted function and resulting parameters are reported in the table 4.

Particles population in size range of 15-30nm are found to be influenced by temperature while particles in the higher size range 150-880nm are affected by higher humidity (Jamriska et al. 2007). The ratio of measured to 1st level of proxy against RH shows a negative correlation (Figure 9). At higher RH (80-100%) coagulation process could be dominant. The coagulation process is responsible for minimizing the number of smaller particles, as these particles coagulate to form bigger particles (Hamed et al. 2011). RH can explain one of the sink terms for the particles population. Thus, RH has been used in the N proxy calculation, and it is representing a sink term for the particles. The relationships between the ratio of measured to 2nd level of particles concentrations proxy against other trace gas and meteorological parameters were tested (not shown here). It was determined that no other variables were improving the proxy significantly. So final N proxy is a function of NO_2 and RH and could be calculated by the equation,

N_{proxy} = Constant * NO_2^{s1} * 10^{RH*s2}. …… (17)

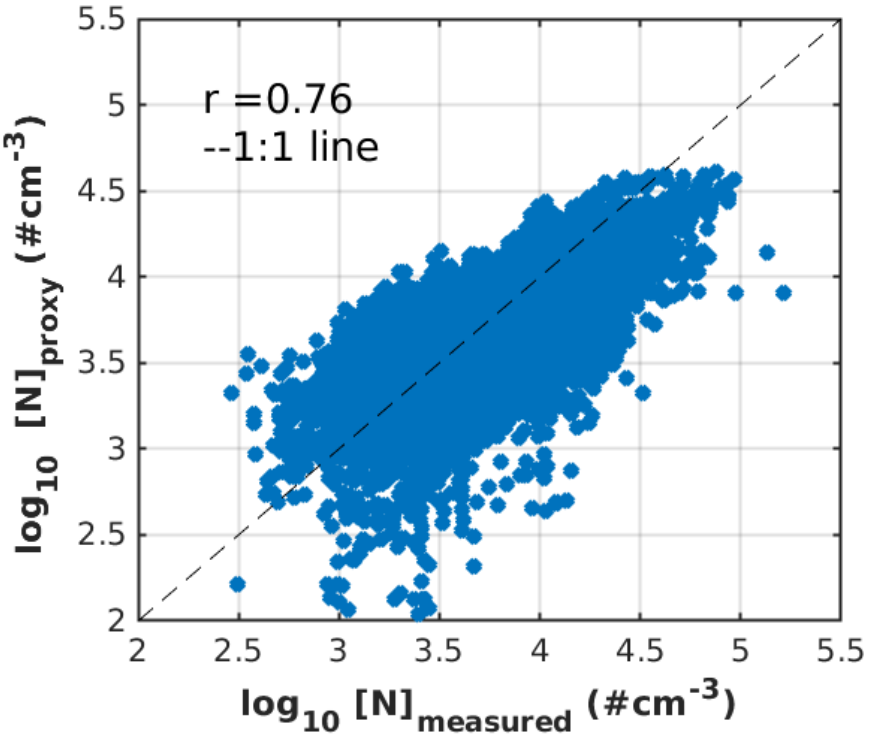

Figure 10: Optimized Particle number concentration proxy as a function of observed Particle number concentration show parameterized NO_2 and RH can be used to predict the Particle number concentration. The resulting uncertainty of using a NO_2 and RH based proxy is reported in table 4.

Initial fitted parameters s1, s2 and the constants were optimized using the MATLAB function fminsearchbnd. The method described in Paasonen et al. 2010 was followed to reduce the variability among the data, and the parameters that yielded the lowest $V_{90/10}$ ratio were taken. $V_{90/10}$ is the ratio of 90^{th} and 10^{th} percentile of the measured to proxy ratio. Final proxy concentration calculated from the optimized parameters against measured concentrations is shown in figure 10. Optimized proxy predicts the measured value strongly (r = 0.76). There is 30% uncertainty related to the proxy calculated data for the analyzed period (2010-2014), and the uncertainty of the data was calculated by the method described in Mikkonen et al. 2011. This uncertainty is acceptable, but whenever a proxy equation is used to describe a hard to measure (or measuring process is expensive or complicated) variable, caution is needed during analysis and interpretation. The first row of the table 4 of N proxy is from 2007-2014. Around later 2010 the NO_2 measurement instrument was upgraded. This could be the factor (the better measurement of NO_2) why uncertainty of 2010-2014 got better compared to the first proxy.

Table 4: Optimized parameters for Particle number concentration (N) proxy. s1, s2 and constants are to be used to approximate N concentrations. $V_{90/10}$ are the values before and after optimization. Uncertainty values tell uncertainty associated with using a proxy instead of measured N concentration. The correlation coefficient between the measured and proxy N is given by r.

Proxy	constant	Slope (s1)	Slope (s2)	$V_{90/10}$ unoptimized	$v_{90/10}$ optimized	uncertainty	r
N (NO_2, RH) 2007-2014	$3.47*10^3$	0.59	-0.0034	2.95	2.92	0.33	0.74
N (NO_2, RH) 2010-2015	$2.94*10^3$	0.60	-0.0035	2.82	2.7593	0.306	0.76

4.4. Condensation sink proxy

DMPS aerosol size distribution data from Kumpula SMEAR III site was used to calculate condensation sink (CS) using equation 1. $PM_{2.5}$ is continuously measured from February 2018 and no DMPS data after July 2018 at the time of this analysis meant the data coverage for this analysis was from Feb 1st – July 31st 2018. Figure 11a shows the condensation sink as a function of $PM_{2.5}$ in 10 base logarithmic scale. A strong correlation between CS and $PM_{2.5}$ was observed. As discussed in the background section, particulate mass distribution is dominated by particles in the accumulation size range, while the surface area distributions of the particles are governed by the larger aitken sizes and accumulation sizes. Thus the positive correlation between CS, a surface area-based parameter, and $PM_{2.5}$ were expected. As particles grow, their mass starts to increase, and their surface area also increases. The interconnection between mass and surface area means $PM_{2.5}$ can be used as a viable variable for proxy. The parameters calculated from the fitted line (figure 11a) gives the first version of condensation proxy ($CS_{proxy,\ 1st}$).

The ratio of measured CS to $CS_{proxy\ ,1st}$ as a function of NO_2 in logarithmic scale shows a positive correlation (Figure 11b). One of the primary sources of particles at the SMEAR III site is traffic. NO_2 is a co-emitted component in the exhaust system along with particles. Considering this fact, NO_2 can be added to the CS proxy, as it partially describes the source of particles.

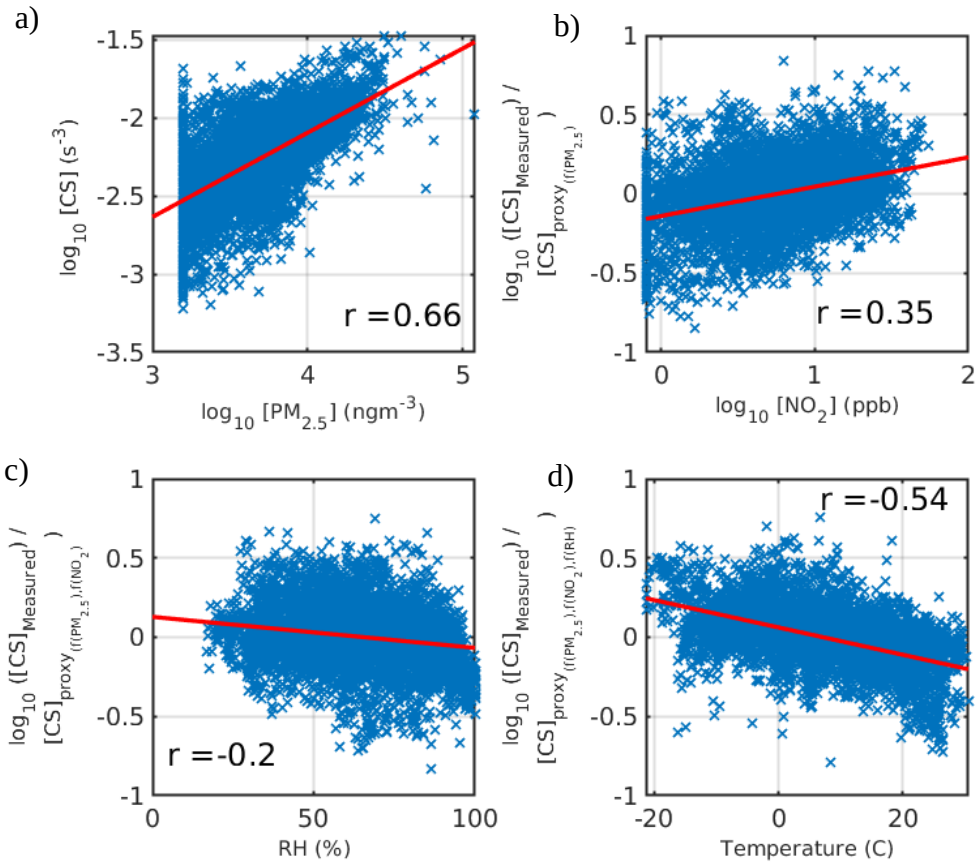

Figure 11: Subplots from top left to bottom right shows the individual steps through which each variable a) $PM_{2.5}$, b) NO_2, c) RH and d) Temperature were added to the CS proxy. The optimized parameters from these fitted functions are reported in the table 5.

The ratio of measured CS to $CS_{proxy\ ,2nd}$ as a function of relative humidity (RH) shows a negative correlation (figure 11,c). Several processes could be responsible for the loss of the particles, which reduces the surface area for the condensable vapour to condense. These could be coagulation or wet deposition process or use (Laakso et al. 2004) of GF (equation 5) in deriving CS (equation 4). At very high humidity coagulation process could be more prevalent, where larger particles are scavenging smaller particles. Also, often new particle formation event associated with low RH conditions (Dada et al. 2017). This could also be true for higher temperature, as the ratio of $CS_{measured}$ and $CS_{proxy\ ,3rd}$ as a function of temperature also shows a somewhat strong dependence of CS on the temperature (Figure 11d). Smaller particles also coagulate to form a more massive particle. In the coagulation process mass is conserved, but the number of particles is not. Particles of smaller sizes

have more surface area compared to the larger sizes at the same mass. RH and temperature both can be added to the proxy to improve the proxy further.

Further, the ratio of $CS_{measured}$ to $CS_{proxy,\ 4th}$ was investigated against wind speed, wind direction and global radiation and these did not show any significant relation, so these were not considered as a variable for proxy. The final proxy with initial parameters was optimized by reducing the ratio of 90^{th} percentile and 10^{th} percentile of the ratio of calculated CS to proxy CS. The optimized proxy equation using $PM_{2.5}$, NO_2, RH and temperature is

$$CS_{proxy} = \text{Constant} * PM_{2.5}^{s1} * NO_2^{s2} * 10^{RH*s3} * 10^{Temp*s4}. \quad \ldots. (18)$$

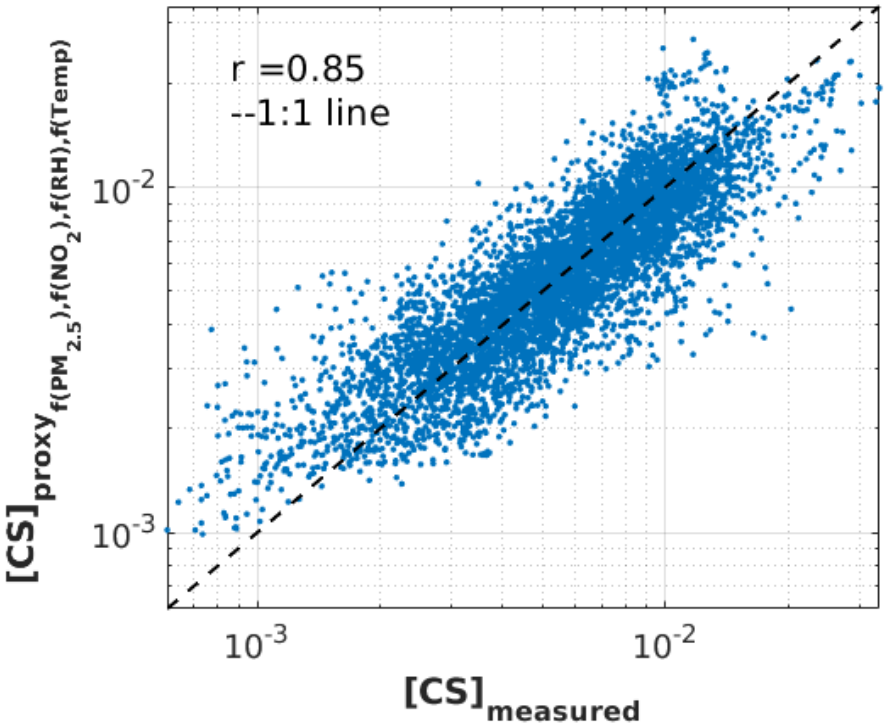

Figure 12: Data points in blue are CS proxy calculated from $PM_{2.5}$, NO_2, RH and temperature as a function of calculated CS and r gives the correlation coefficient between them.

The optimized CS proxy plotted against the calculated CS shows (Figure 12) proxy using $PM_{2.5}$, NO_2, RH and temperature are approximating the concentrations nicely (figure 12). Proxy calculated using BC, RH and temperature also performs similarly (Table 5). But the AQT 420 sensors can not measure BC means the use of BC was not in the final consideration. CS proxy (Table 4) derived using BC proxy (derived later, calculated using $PM_{2.5}$, NO_2), predicts the higher CS values slightly

better compared to the CS proxy derived using $PM_{2.5}$, NO_2, RH and temperature (not shown here), though both line 1 and line 3 proxy (table 5) uses same variables, only changes are in the proxy parameters and constant. Comparison between the measured BC and proxy BC was done to see how BC proxy is working compared to measured BC in predicting CS. Similar results means BC proxies can be used as a substitute for measured concentrations. All proxies (table 5) have similar uncertainties associated with them.

Table 5. s1, s2, s3, s4, and constants are to be used to approximate CS concentrations. $V_{90/10}$ are the values before and after optimization. Uncertainity values tell uncertainity associated to using a proxy instead of calculated CS value from DMPS data. Correlation coefficient between the calculated and proxy CS is given by r.

Proxy	constant	Slope (s1)	Slope (s2)	Slope (s3)	Slope (s4)	V (90/10) unoptimized	V (90/10) optimized	uncertainty	r
CS ($PM_{2.5}$, NO_2, RH, Temp)	2.98e-05	0.44	0.29	-0.005	-0.011	2.44	2.19	0.24	0.85
CS (BC, RH, Temp)	3.60e-5	0.62	-0.0065	-0.0135		2.78	2.39	0.24	0.84
CS (BC_{proxy}, RH, Temp)	1.38e-5	0.83	0.012	-0.0052		2.30	2.228	0.24	0.85

4.5. Black carbon proxy

Along with SMEAR III site (Kumpula) in Helsinki metropolitan area, BC is measured at Mannerheimintie, Mäkelänkatu and Tikkurila (traffic site), Kallio (urban background), Lukki (rural environment) and Itä-Hakkila (Small-house area with wood combustion and traffic). Helsinki Region Environmental Services Authority (HSY) conducts the measurements at these locations along with some other sites around the Helsinki metropolitan area (HAQT deliverable 1.3) except SMEAR III. Individual BC proxies based on the data from Kumpula, Mäkelänkatu and Itä-Hakkila were made, and their performance as a stand-alone proxy was analyzed by applying them to the rest of data from the locations mentioned above (results are shown later). Further, those results were compared to the proxy calculated from a combined data-set from three locations with variable environmental condition. It was determined that combined proxy performs better in almost all sites and lowers the uncertainty of using a proxy to predict BC concentrations.

Combined proxy was derived from the data set of Kumpula, Mäkelänkatu and Ita-Hakkila site. Data from 2018 was used for the analysis. The scatter plot of BC against $PM_{2.5}$ shows a significant relation (r = 0.63) among them (figure 13a). The 80-300nm size range particles dominate BC size

distribution, which falls in the accumulation size range, and particles in the accumulation mode size range dominate $PM_{2.5}$. $PM_{2.5}$ is an ideal first variable for the BC proxy.

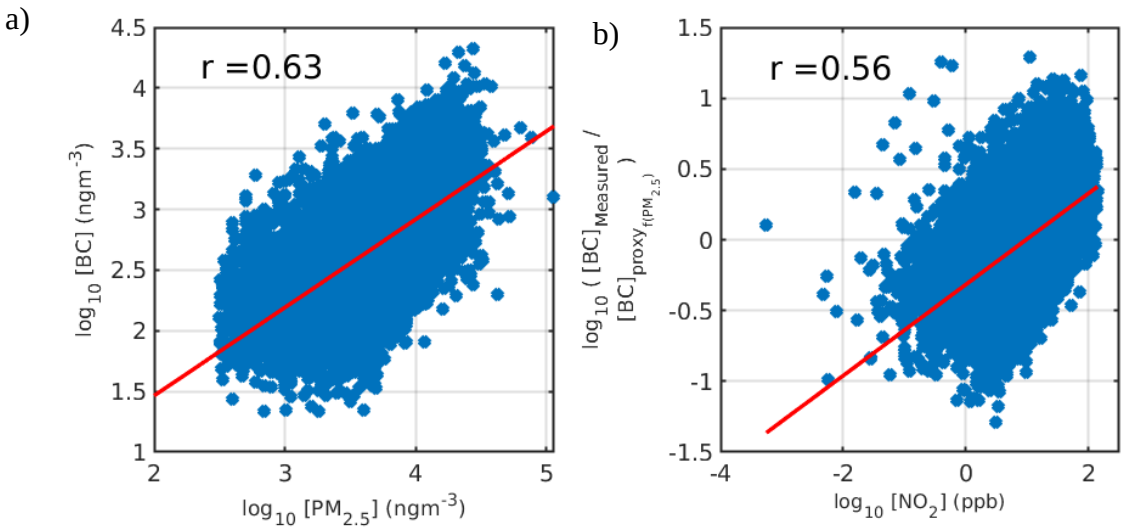

Figure 13: A combined dataset from Kumpula, Mäkelänkatu and Ita Hakkila were used to calculate the BC proxy. a) measured BC as a function of measured $PM_{2.5}$ is shown on the left. b) The ratio of measured BC to the first version of proxy $BC_{proxy,\ 1st}$ plotted as a function of NO_2 is shown on the right. The associated parameters to the fitted functions are reported in table 6.

Combustion processes produce a significant proportion of the atmospheric NO_2, and BC is also a product of incomplete combustion of fossil fuel and wood-burning. Considering their somewhat similar sources, it is natural that NO_2 and BC show significant association with each other (figure 13b). The approximation of BC concentrations improved considerably with the addition of NO_2. Other variables (wind speed, direction, temperature and RH) were tested to develop the proxy further, but none showed a significant impact in the proxy construction. The final BC proxy, using $PM_{2.5}$ and NO_2, were optimized using the method (Paasonen et al. 2009), and the optimized proxy has the form,

$$BC_{proxy} = constant * \left(PM_{2.5}^{s1} * NO_2^{s2} \right) \quad \ldots. (19)$$

Proxy based on combined dataset performs well (figure 14) with the measured concentration, though the proxy underestimates higher BC values.

Table 6. Optimized parameters for BC proxies from individual sites (Mäkelänkatu, Ita-Hakkila and Kumpula) and combined data set (of those three places) are given here. s1, s2 and constants are to be used to approximate BC concentration of a particular location. $V_{90/10}$ are the values before and after optimization. Lower uncertainty value means proxy is performing better (in percentage, here 28-44%). The correlation coefficient between the measured and proxy is given by r.

Proxy	constant	Slope (s1)	Slope (s2)	$V_{90/10}$ unoptimized	$V_{90/10}$ optimized	uncertainty	r
Combined	5.70	0.42	0.41	4.19	3.67	0.39	0.80
Mäkelänkatu	1.69	0.41	0.78	3.28	2.59	0.28	0.89
Itä-Hakila	2.81	0.44	0.63	4.22	3.99	0.44	0.77
Kumpula	10.73	0.36	0.43	3.66	3.30	0.35	0.81

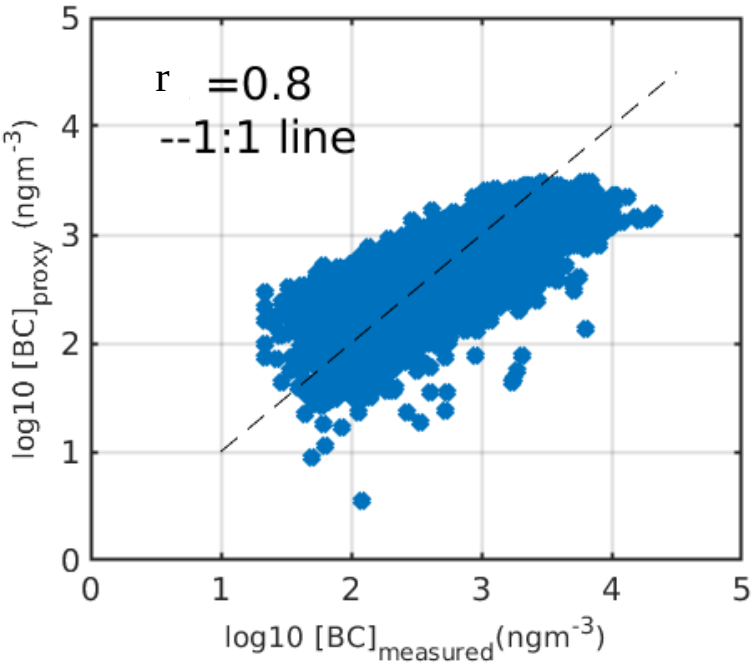

Figure 14: Final optimized combined BC proxy as a function of measured BC for the combined data set shows nice agreement between proxy and measured data (r = 0.8). Dashed line is the 1:1 line.

Parameters (s1) related to $PM_{2.5}$ does not vary (0.36-0.44) that much (table 6), but parameters (s2) related to NO_2 varies quite a lot (0.43-0.78). Highest factor (for NO_2) being at Mäkelänkatu, a street canyon site, where pollution is dominated by traffic. Lowest uncertainty is also associated with this location, along with the highest correlation coefficient. On all proxies, $V_{90/10}$ decreases after optimization, which is to be expected (Paasonen et al. 2009).

Proxy parameters for combined proxy from table 6 were applied to the individual data from Kumpula, Itä-Hakkila and Mäkelänkatu, and time series of proxy and measured concentrations are shown in figure 15. High BC values are underestimated in Kumpula, but Itä-Hakkila and Mäkelänkatu high values are less underestimated. But for those two places, lower BC values are often overestimated. Proxy captures the seasonal and daily trends well.

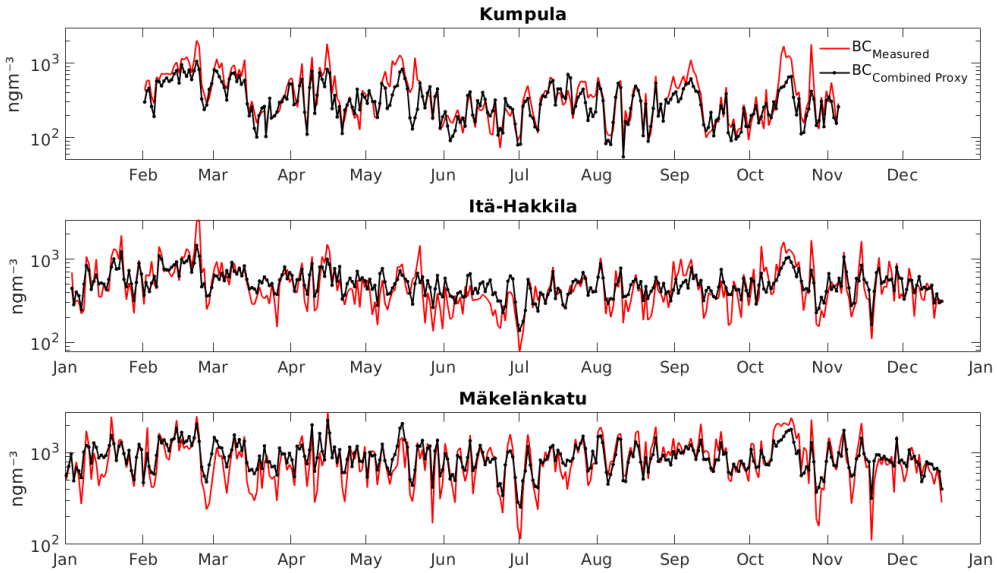

Figure 15: Individual time series of measured and proxy BC concentrations at urban background (Kumpula), small house area (Ita-Hakkila) and road side (Makelankatu). Proxy concentrations were calculated using parameters for the combined data.

The optimized parameters for proxies were used to data from additional sites to calculate BC proxy concentrations at those sites (supplementary figure 2,3 and 4). It was done to compare them to the actual measured BC concentrations and evaluate the performance of the proxy. The sites reflected different environments like traffic sites (Mannerheimintie, Mäkelänkatu, Tikkurila), urban (Kallio, Kumpula) and rural (Luukki) background environment, and small house residential area (Itä-Hakkila). Testing for different locations gives a proper perspective on how the proxy will perform in different environments.

Two urban background site (Kumpula and Kallio) does not show that much difference in terms of correlation coefficient r (table 7). Although traffic sites Mäkelänkatu and Tikkurila are similar, the other traffic site Mannerheimintie is much different compared to those two locations. This could be related to the dispersion of pollutants on those locations. And also to the meteorological conditions

like particular frequent wind direction, and urban road infrastructure, dominating pollutants behaviour (Pirjola et al. 2005).

Table 7: Correlation between the measured and proxy concentrations are given below. Four different sets of proxy parameters (location mentioned on the first column) from table 6 were used for this analysis and was used to the individual location's data mentioned on the first row.

Proxy	Kumpula	Mäkelänkatu	Itä-Hakila	Kallio	Luukki	Mannerheimintie	Tikkurila
Kumpula	0.82	0.88	0.76	0.83	0.81	0.79	0.89
Combined	0.81	0.86	0.76	0.82	0.81	0.78	0.88
Mäkelänkatu	0.79	0.89	0.76	0.82	0.81	0.80	0.89
Itä-Hakkila	0.80	0.88	0.76	0.83	0.81	0.80	0.89

BC, as a function of $PM_{2.5}$ and NO_2, is also different (r values, supplementary figure 1) for Mannerheimintie compared to Mäkelänkatu and Tikkurila. A similar analysis for other locations is also shown in supplementary figure 1. Even though there is very little change in r values for different proxies, proxy parameters make subtle changes to the data points around 1:1 line (supplementary figure 2). Where, for example, the parameters from combined proxy perform better compared to the parameters obtained from Kumpula data in centering the data points around 1:1 line. Supplementary figure 3 and 4 shows similar deviations of datapoints around 1:1 line with the use of Mäkelänkatu and Itä-Hakkila proxies, respectively.

Table 7: The ratios ($V_{90/10}$) of 90th percentile to 10th percentile of the ratio of measured to proxy concentrations for the four different proxies (1st column) for individual locations (1st row).

	Kumpula	Makelankatu	Ita-Hakkila	Kallio	Tikkurila	Manneheimentie	Lukki
Kumpula	3.30	3.30	4.25	3.44	3.32	3.46	4.38
Makelankatu	4.84	2.59	4.41	3.25	2.64	2.99	4.45
Ita-Hakkila	3.87	2.73	3.99	3.12	2.71	3.09	4.03
Combined	3.35	3.29	4.26	3.42	3.25	3.43	4.38

Four different sets of proxy parameters produced four different sets of $V_{90/10}$ values. These difference could be related to the meteorological conditions, pollutant emission sources and spatial distribution of the pollutants. It still can not be determined which proxy is better though Kumpula and combined $V_{90/10}$ values were almost similar. Uncertainty study shows that proxy derived from the combined dataset has more excellent usability compared to a proxy-based dataset of a particular place.

The subtle changes involving proxy parameters became much more evident when uncertainty analysis was performed. Uncertainties associated with proxies developed from individual sites varied broadly (28% - 69%), but that got reduced (33% -50%) when combined data set was used (Table 9). This shows the importance of additional data from different sites while constructing proxy variables. There is a high uncertainty involved in using proxy parameters calculated from only one place compared to the uncertainty associated with proxy parameters which were constructed using data from different environments. Data from different conditions will have much more spatial variability compared to the data from only one place. Thus caution needs to be implemented when using proxy parameters calculated from a specific type of condition.

Table 9: The uncertainty values describe the performance of the proxy, with the lower values describing the least uncertainty for that proxy in predicting the measured value.

Proxy	Kumpula	Mäkelänkatu	Ita Hakila	Kallio	Luukki	Mannerheimintie	Tikkurila
Kumpula	0.35	0.38	0.48	0.69	0.68	0.65	0.42
Mäkelänkatu	0.59	0.28	0.51	0.35	0.42	0.42	0.31
Itä-Hakkila	0.41	0.38	0.44	0.58	0.44	0.69	0.36
Combined	0.39	0.33	0.46	0.48	0.50	0.46	0.36

4.6. Lung deposited surface area proxy

In this analysis, the diffusion current from the Pegasor AQ Urban instrument was used. The method describing parameterization of the diffusion current to approximate the LDSA concentrations is given by Kuula et al. 2019. In this study, we do not use parameterization for the Pegasor AQ Urban diffusion current. The diffusion current itself was used directly and levelled as $PAQDC_{LDSA}$ concentration in data analysis and figure levels, respectively. Lung deposited surface area (LDSA) concentrations are mainly derived from the DMPS size distribution data. The calibrated total current of the electrical low-pressure impactor (ELPI) (Kuuluvainen et al. 2016), and diffusion current of Pegasor AQ Urban, DiSCmini, and Partector (Kuula et al. 2019) instruments are also found to represent the LDSA concentrations calculated from the reference DMPS to a reasonable accuracy.

As shown earlier in figure 4, the Particle number concentration at the SMEAR III is dominated by the particles from nucleation, aitken, and accumulation mode size range. Also mentioned earlier is, NO_2 is co-emitted during the combustion process. Inclusion of NO_2 in the $PAQDC_{LDSA}$ proxy is justifiable for the derivation of the $PAQDC_{LDSA}$ proxy ($r = 0.75$, figure 17a), as NO_2 is a good pollution indicator for particle number concentrations.

In urban background areas $PM_{2.5}$ mass is typically dominated by the accumulation mode particles (Timonen et al. 2018). Particles mass concentration is dominated by the particles in the accumulation mode size range (figure 4). Pegasor AQ urban instrument diffusion current plotted as a function of $PM_{2.5}$ shows a strong correlation between them (not shown here). Similar results have been observed, by Kuuluvainen et al. 2016 for most of the environment and the level of the association depends on the type of environment, and by Kuula et al. 2019 using low-cost sensors. Contribution of both volatile and non-volatile mass in the lung health effects is described in section 2.7 along with the importance of the particles from the nucleation and accumulation mode size range. Contribution of particles in the nucleation mode and accumulation mode towards the LDSA size distribution was observed at traffic sites, and contribution from the long-range transported aerosol in residential areas was seen around Helsinki (Kuuluvainen et al. 2016). Saarnio et al. 2012 reported that woodburning contributes significantly towards the $PM_{2.5}$ in cold seasons in both urban and suburban areas to a certain degree. Still,the effect of woodburning towards LDSA concentrations is minimal (Kuuluvainen et al. 2016). Observed results in figure 17a and 17b, and supporting knowledge from the literature illustrates NO_2 and $PM_{2.5}$ being ideal variables for the inclusion in the $PAQDC_{LDSA}$ proxy**.**

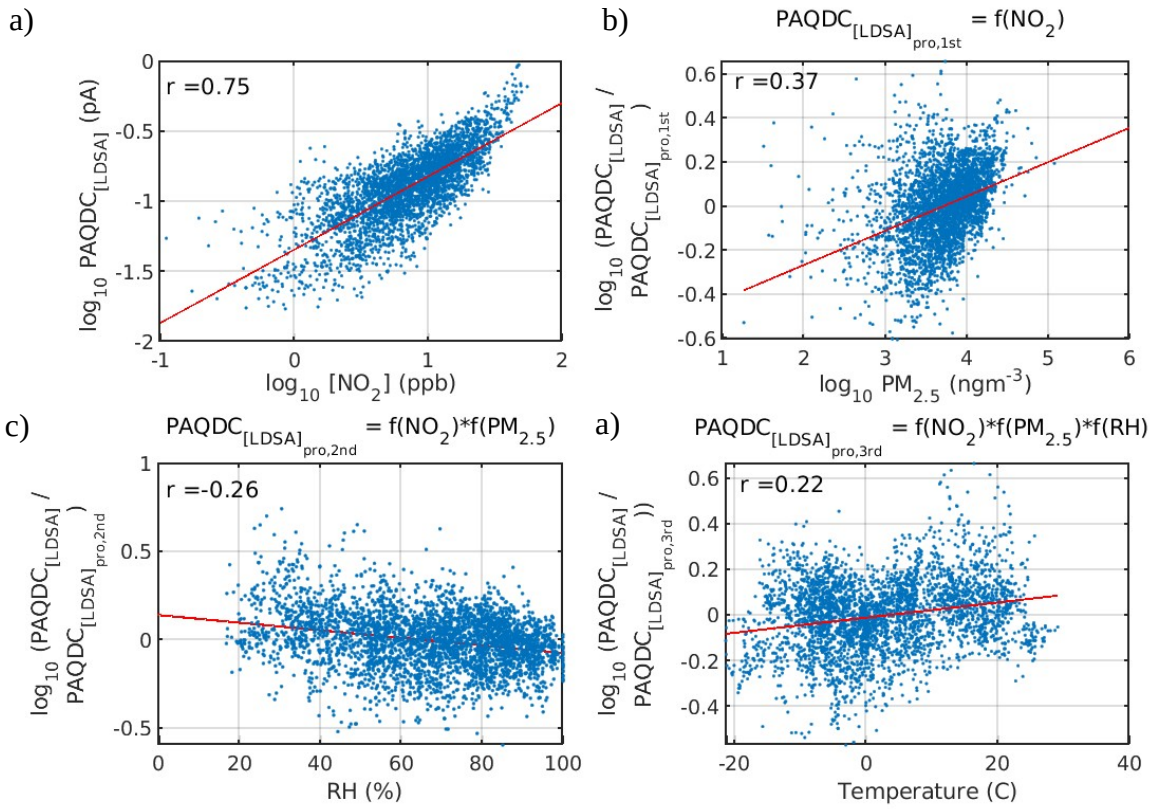

Figure 17: *P*egasor *AQ* urban instrument *D*iffusion *C*urrent (PAQDC) leveled as $PAQDC_{LDSA}$. $PAQDC_{LDSA}$ as a function of NO_2 (17a), The ratio of $PAQDC_{LDSA}$ to 1st level $PAQDC_{LDSA,proxy}$ as a function of $PM_{2.5}$ (17b), the ratio of $PAQDC_{LDSA}$ to 2nd level $PAQDC_{LDSA,proxy}$ as a function of *r*elative *h*umidity (RH) (17c) and the ratio of $PAQDC_{LDSA}$ to 3rd level $PAQDC_{LDSA,proxy}$ as a function of temperature (17d) shows the individual steps for the proxy construction. The optimized parameters calculated for these variables to be used in the final $PAQDC_{LDSA,proxy}$ are given in the the table 10.

Further investigation on how $PAQDC_{LDSA}$ proxy can be improved led to the inclusion of, RH figure17.c, and temperature figure 17.d. Reche et al. 2015 reported the influence of both traffic and nucleation events towards the increase of LDSA concentrations. A clean, cloudless environment is thought to be important for the nucleation events, and temperatures higher than 25°C and lower than -21° C are also not favourable for nucleation to occur (Dada et al. 2017). At higher temperature, more monoterpenes and biogenic organic compounds are released to the atmosphere. Photochemically produced oxidation products (Peräkylä et al. 2014, Kontkanen et al. 2016) are also responsible for the particle formation (Ehn et al. 2014) and growth of particles (Paasonen et al. 2013) along with sulfuric acid (Paasonen et al. 2010, Paasonen et al. 2009, Petäjä et al. 2009).

Lower RH is suitable for nucleation events (Hamed et al. 2011) and the influence of RH could be more of photochemical nature through cloudiness (Dada et al. 2017). Strong relation between RH and trace gases like SO_2 and O_3 are observed, these gases regulate the production of precursor vapours that are needed for nucleation to occur (Dada et al. 2017, reference therein). Further, The performance of the pegasor urban air quality instrument somewhat also related to the operating temperature and relative humidity (Kuula et al. 2019 and reference therein). That may also explain the inclusion of RH and temperature for making the proxy better. After optimization, the proxy with all the relevant parameter can be written as,

$$PAQDC_{LDSA,proxy} = \text{Constant} * NO_2^{S2} * PM_{2.5}^{S1} * 10^{RH*s4} * 10^{temp*s4}. \quad \ldots. (20)$$

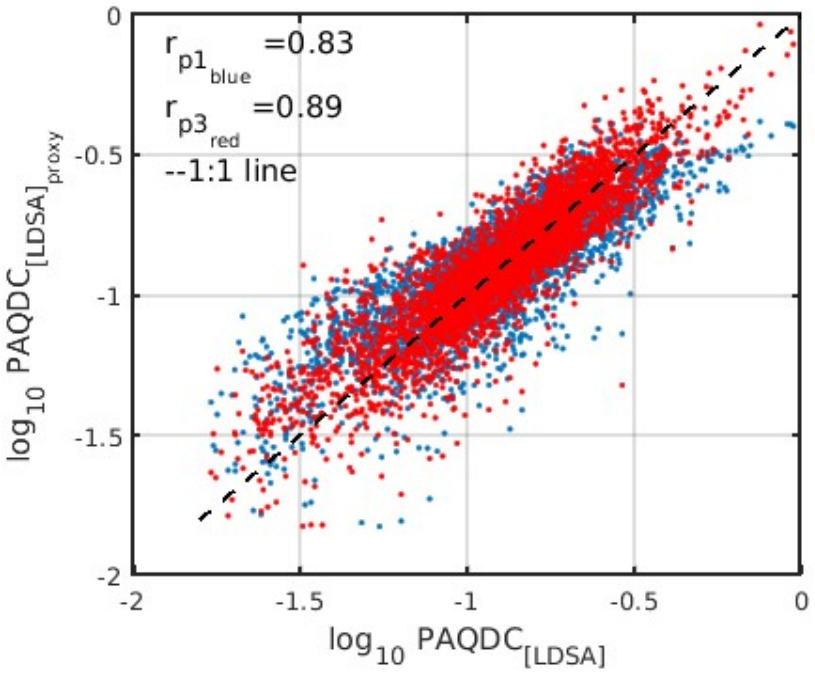

Figure 18: $PAQDC_{LDSA}$ proxy versus measured $PAQDC_{LDSA}$ show the performance of $PAQDC_{LDSA}$ proxy (p_3, N, $PM_{2.5}$, temperature and RH, red dots) calculated with Particle number concentration (N) compared to proxy (p_1, NO_2, $PM_{2.5}$,RH and temperature, blue dots) without N. Data coverage February 2018 - May 2018. Similar comparison between the $PAQDC_{LDSA}$ proxy p_1 and p_2 is shown in the supplementary figure.

P_3 proxy data centers around the 1:1 line nicely compared to the p_1 proxy data (figure 18). The correlation coefficient for p_3 is also high (Table 10) compared to p_1. These are also true for the p_2 proxy when compared to the p_1. But proxies p_2 and p_3 both use Particle number concentration (N) as

one of the predictor variables. Accurate measurements of N requires complex measurement setup and rather expensive reference instruments, thus making the use of N as a proxy variable not viable. This similar argument is also valid for CS (p_6, table 10), as it is a product of aerosol size distribution data. But here CS data was used for one of the proxies as CS data was available for the whole period when pegasor air quality instrument was operational at the SMEAR III site.

Measurement of BC is also complicated and not that viable for being used in proxies. Still, tests were done to see how BC performs in predicting the $PAQDC_{LDSA}$ (Table 10) because BC data from the SMEAR III site was available for the analysis period. The uncertainties associated with these $PAQDC_{LDSA}$ proxies are low (table 10). For example, 24% for the p_1 proxy, which uses the NO_2 as an indicator for traffic or combustion contribution. The p_7 proxy (Table 10) was looked at because of the available N data from the SMAER III site, and also it allowed to look at the whole year $PAQDC_{LDSA}$ data. Measured N data from accurate, non-expensive and less complicated instrument could be used in the future in case of such devices becomes readily available. A similar argument can also be true for p_2 and p_3 proxies.

Table 10: Optimized parameters for the variables used in the $PAQDC_{LDSA}$ proxy. The uncertainty value describe the performance of the proxy, with the lower values describing the least uncertainty for that proxy in predicting the measured value. The proxy versions ($PAQDC_{LDSA\ p1\text{-}p7}$) given in one of the column are used to describe time series plots (figure 20 and 21).

Proxy	constant	Slope (s1)	Slope (s2)	Slope (s3)	Slope (s4)	V (90/10) unoptimized	V (90/10) optimized	uncertainty	R	Proxy Version (PAQDC (LDSA))
$LDSA_{Short}$ (NO_2, $PM_{2.5}$, RH, Temp)	0.0097	0.44	0.22	-0.0010	0.0044	2.35	2.27	0.24	0.83	P1
$LDSA_{Short}$ ($PM_{2.5}$, NO_2, N, Temp)	1.34e-04	0.29	0..166	0.475	0.0069	2.08	1.85	0.19	0.90	P2
$LDSA_{Short}$ (N, $PM_{2.5}$, Temp, RH)	1.36e-4	0.704	0.33	0.0084	0.0021	1.95	1.89	0.19	0.89	P3
$LDSA_{Short}$ (BC, NO_2, Temp)	0.0055	0.40	0.28	0.0036		2.23	2.10	0.22	0.86	P4
$LDSA_{long}$ (CS, RH, N, Temp)	1.5444	0.81	-0.0051	0.28	-0.0043	1.487	1.456	0.11	0.975	P6
$LDSA_{long}$ (N)	1.1e-04	0.79				3.13		0.33	0.77	P7

Both LDSA and CS are derived from the DMPS aerosol size distribution data. Both these parameters describe surface area properties of aerosol particles. $PAQDC_{LDSA}$ is found to correlate strongly with CS (Figure 19), and $PAQDC_{LDSA}$ is parameterized to calculate LDSA concentrations (Kuula et al. 2019).

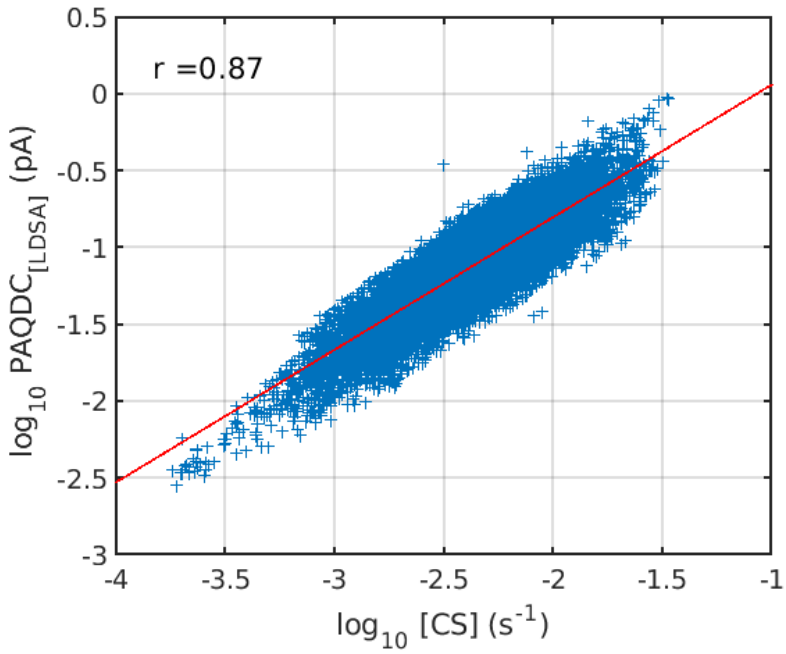

Figure 19: pegasor air quality diffusion current (PAQDC) as a function of condensation sink derived from DMPS aerosol size distribution data.

Data from June 2017 to May 2018 were analyzed to investigate seasonal trends in $PAQDC_{LDSA}$. The median concentration of the $PAQDC_{LDSA}$ as a function of the months shows two high concentrations peaks during February and May (figure 20). The corresponding aerosol size distributions and Particle number concentration were analyzed (few example days of that analysis are shown in section 4.2). The size distribution show two different patterns over the two months. In February, particles in the smaller diameter range are more prevalent and are generally considered to be traffic emitted particles. Particles, in this case, are either formed in the exhaust or formed in the exhaust dilution process in the ambient condition immediately after exiting the tailpipe. Median particles number concentration (N) also show the highest peak in February.

From the end of January onwards until the end of March on 2018 weather over Finland was dominated by high pressure systems, and prolong cold period as a result of sudden tropospheric warming (Karpechenko et al. 2018). The much higher $PAQDC_{LDSA}$ during that period showed less day-night variability compared to any other months (figure 21). The effect of often sunny and stable condition on new particle formation during that period or the meteorological conditions (e.g. lower

boundary layer) governing the pollution dispersion or distribution at the same time could explain the observed behaviour of the pollutants, but this was not the scope of this analysis. Few example days where new particle formation event was prevalent was shown in section 4.2.

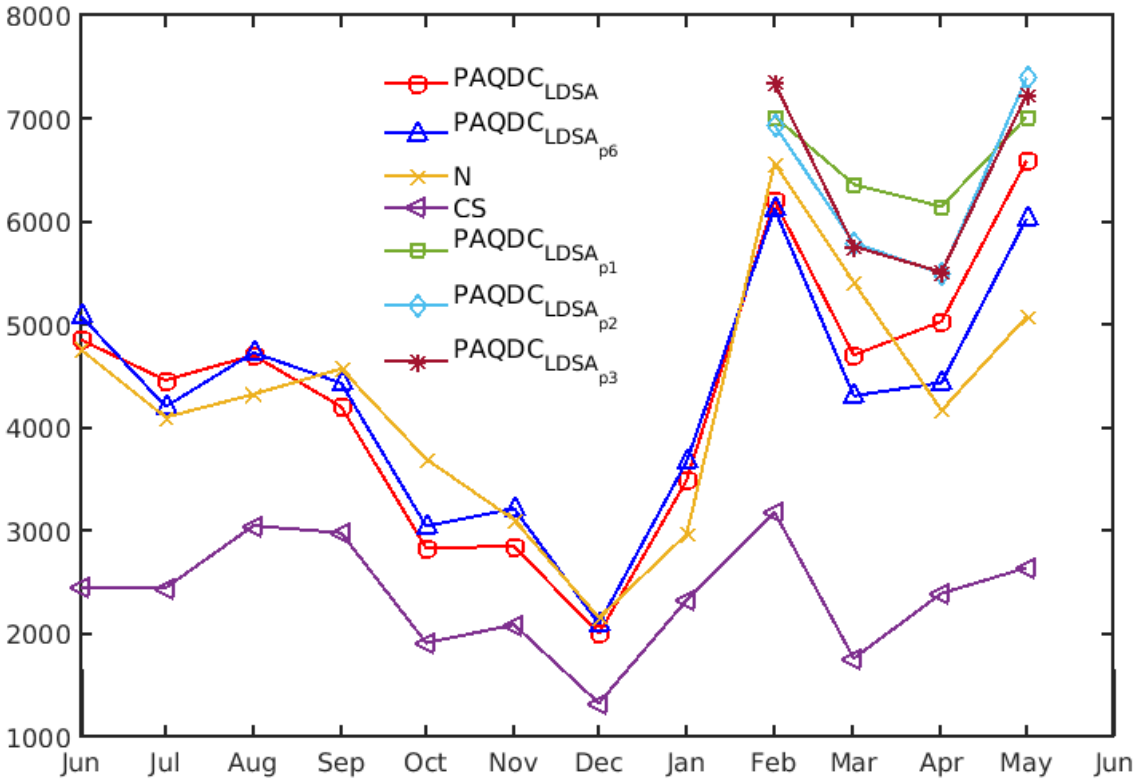

Figure 20: Monthly median values of several parameters. Values of the parameters in figure are scaled by $PAQDC_{LDSA}$ * $50*10^3$, N remained same and $CS*500*10^3$.

In May, particles in the smaller size range are not visible all the time, but on many occasions, particles in the 50 – 150 nm size range are more prevalent (An example day was shown in section 4.2). Particles in this size range could be associated to the long-range transported particles (Hussain et al. 2008) originated from the cleaner rural environment in the north, or aged traffic particles originated in the urban area itself and got transported to the measurement site. These long-range particles can scavenge the smaller traffic particles or newly formed particles quite efficiently and preventing the measurement of the smaller particles and which may explain the non-measured smaller particles in the size distribution data (Hussain et al. 2008). So even though the Particle number concentration is lower in May compared to March, slightly larger particles in May are responsible for the equivalent surface area contribution compared to March, hence similar $PAQDC_{LDSA}$ readings for both months.

Often particles are seen to grow from smaller sizes to larger sizes within the 50-150nm size range not shown here or in section 4.2. The scavenging of the smaller particles could explain the slight growth of the particles. And also, by growth related to the ageing of the traffic particles and. The temperature was a record high during May over the southern Finland region (FMI news release, https://en.ilmatieteenlaitos.fi/press-release/539036550) and during high-temperature conditions particle growth has also been observed to be associated with condensation of organic vapours (Paasonen et al. 2013). During these growth periods, $PAQDC_{LDSA}$ concentrations are found to increase (not shown here), but the $PAQDC_{LDSA}$ concentrations remain steady when particles in a particular size range remain constant for a long time without change to their size range.

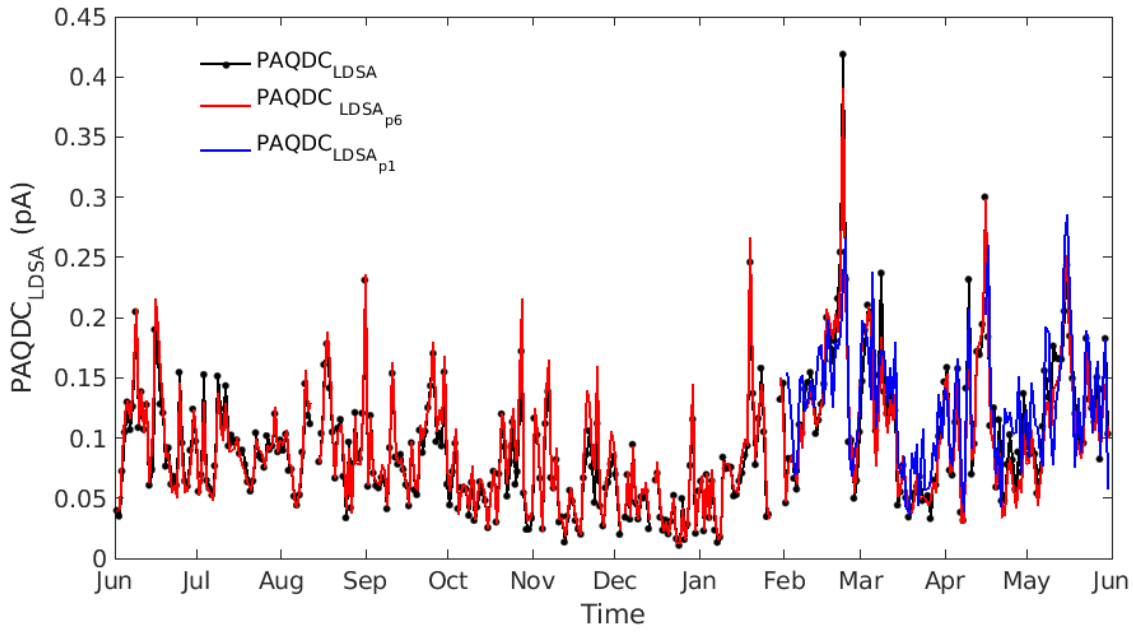

Figure 21: Daily median values of measured and proxy pegasor air quality diffusion current (PAQDC).

While three different size classed (2-10nm, 10-50nm, and 50-250nm) Particle number concentration showed strong correlation with $PAQDC_{LDSA}$ for an example day on February 5th (not shown here), Particle number concentration for the 2-10nm size range did not show the similar result during March 26th -28th. Or on May 5th (table 11).

Table 11: Correlation coefficient (r) values for the relation between Particle number concentration (N) among different size class and $PAQDC_{LDSA}$.

	$PAQDC_{LDSA}$ (February 5th)	$PAQDC_{LDSA}$ (March 26-28th)	$PAQDC_{LDSA}$ (May 12th)
N_{2-10}	0.81	0.12	0.0067
N_{10-50}	0.91	0.79	0.83
N_{50-250}	0.77	0.91	0.96

5. Conclusions

Proxy concentrations were derived for black carbon (BC), condensation sink (CS), pegasor AQ urban diffusion current ($PAQDC_{LDSA}$) and Particle number concentrations (N). Additional proxy for sulfuric acid (SA) was also developed. For BC, only $PM_{2.5}$ and NO_2 were enough to derive a reliable proxy (correlation coefficient, r = 0.80), and the addition of any other parameter did not improve the proxy. For combined BC proxy, data from three sites were used, which helped to include the different meteorological and environmental conditions associated with individual sites—and thus creating a better picture for the often changeable spatial characteristics of the urban environment. Applying derived proxy to several other locations helped in evaluating the usefulness of the proxy by comparing the measured and proxy concentrations. The uncertainty associated with using a proxy is evaluated through uncertainty analysis, which calculates the correctness of proxy concentrations instead of measured values. Proxy derived using combined data reduced the associated uncertainty range (33-50%) of using proxy concentrations compared to any other individual site (35-69%, 28-59%, or 36-69%) based proxy. Thus, it was seen that it is useful to add data from multiple locations for proxy construction, as this will ensure different environmental

conditions are taken into account. Otherwise, it is necessary to apply caution when using a proxy that is only being developed from data for one location. For the urban environment, the discretion should be more adhered to, as conditions in these sites are rapidly changeable. In section 4.2, some example cases show different environmental conditions that affect the SMEAR III site. Whether this case studies will help to validate the proxy further and improve the proxies of this study, was not investigated any further as this was not the goal of this analysis and will probably need additional work in the future.

For CS and $PAQDC_{LDSA}$, use of $PM_{2.5}$, NO_2, RH and temperature yielded reliable proxies (correlation coefficient, r = 0.85 and 0.83, respectively). For Particle number concentration, NO_2 and RH gave a simple proxy that has a strong correlation (r = 0.76). Additionally, a campaign data for SA from SMEAR III site used to produce a proxy for SA. SO_2, Global radiation, CS and RH gave the best version of that proxy. Proxy for SA was also previously derived for the SMEAR II site. Proxy developed in this study is performing similarly to the proxy of the SMEAR II site or proxy obtained by Mikkonen et al. 2011. Mikkonen et al. 2011 proxy is based on multiple sites and includes more information about different environmental conditions. SA proxy had a correlation coefficient (r) of 0.85. All of the expressions for proxies for SA, N, CS, BC and $PAQDC_{LDSA}$ can be found from the equations 16-20, and the associated parameters and constants can be seen from the table 2, 4, 5, 6, and 10, respectively. Using the measured AQT 420 data to implement these proxies at air quality network will give additional parameters for air quality monitoring systems, helping to build a dense network.

6. Supplementary figures

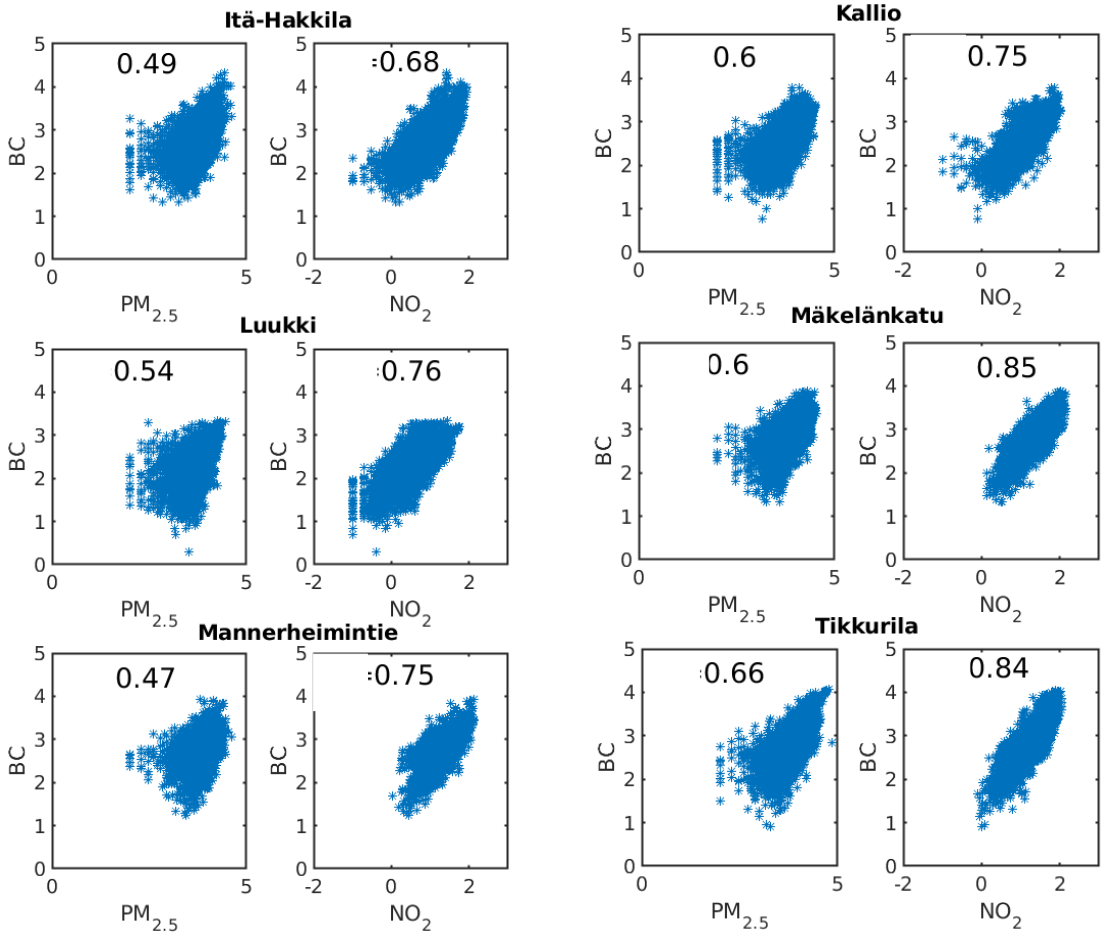

Supplementary figure 1: BC as a function of $PM_{2.5}$ and NO_2 at the individual stations. The data was measured over the whole year of 2018. BC shows much stronger correlation with NO_2 (r = 0.68-0.85) compared to the $PM_{2.5}$ (r = 0.47-0.66) .

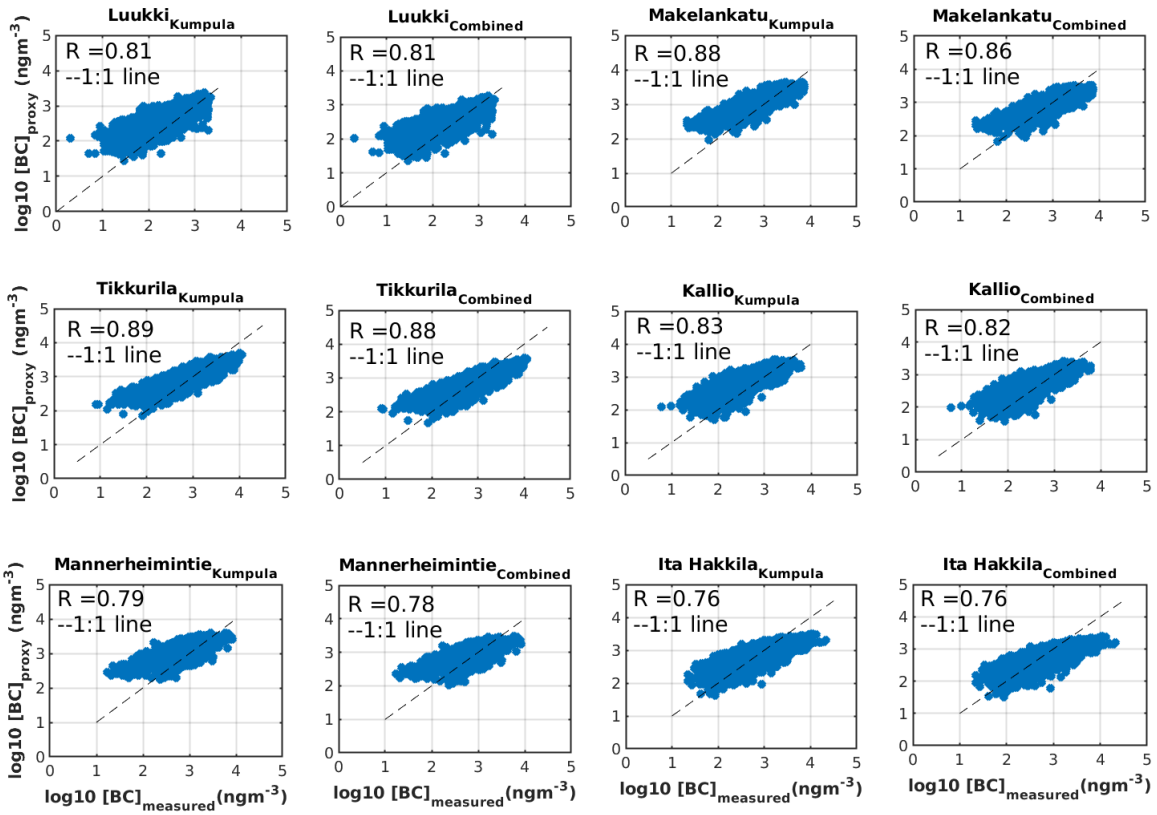

Supplementary figure 2: BC proxy testing: $PM_{2.5}$ and NO_2 were used from Kumpula data to produce a Kumpula based BC proxy. Kumpula and combined BC proxy were used to test the performance of the proxies at other locations. Slight changes in the correlation coefficient values, and the position of the 1:1 line through the data were observed. Often data centers around the 1:1 line for the proxy concentrations based on parameters from the combined proxy compared to the Kumpula based proxy concentrations.

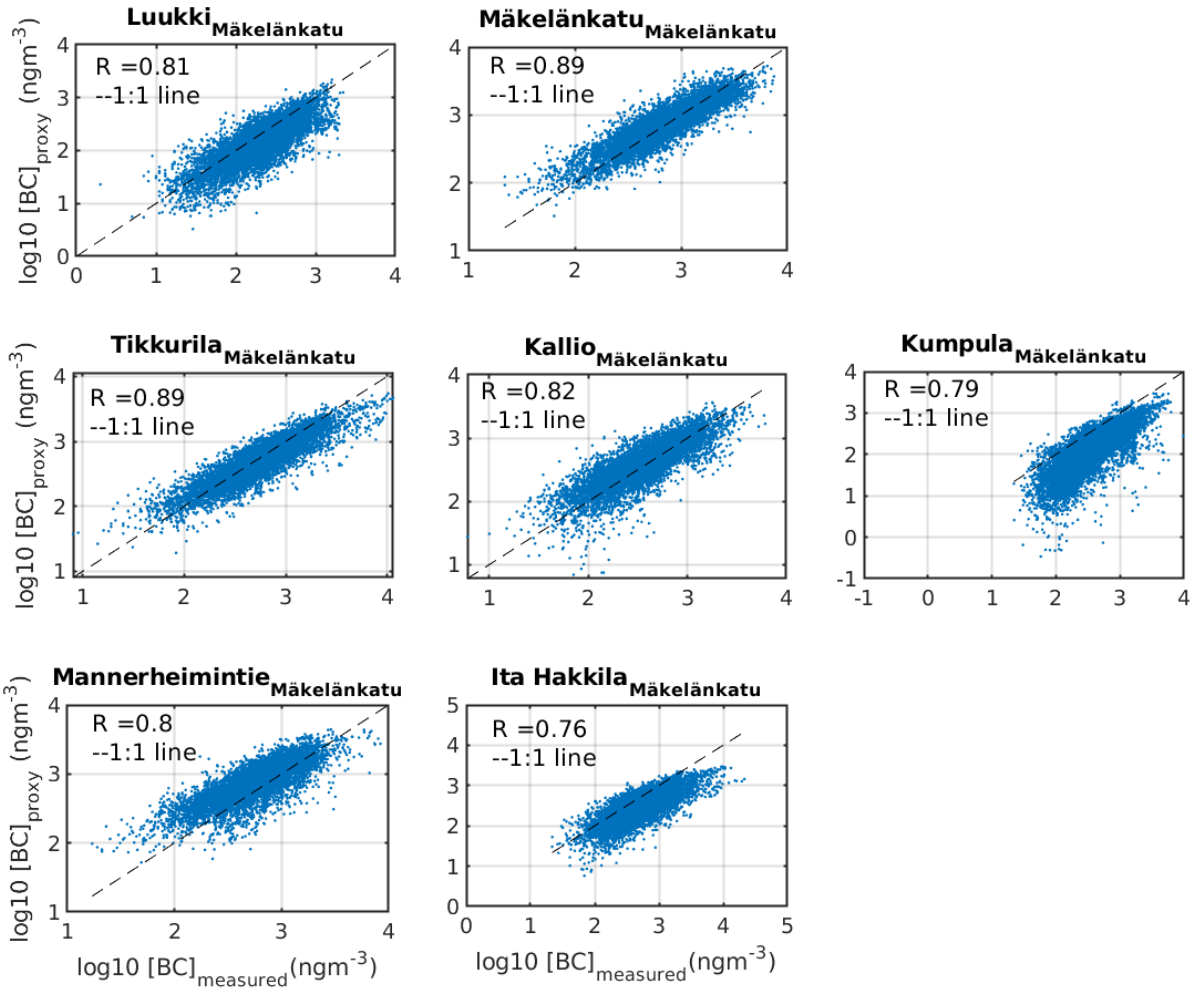

Supplementary figure 3: Proxy concentrations based on the Mäkelänkatu proxy parameters often resulted in large variations in the placement of the 1:1 line compared to the supplementary figure 2.

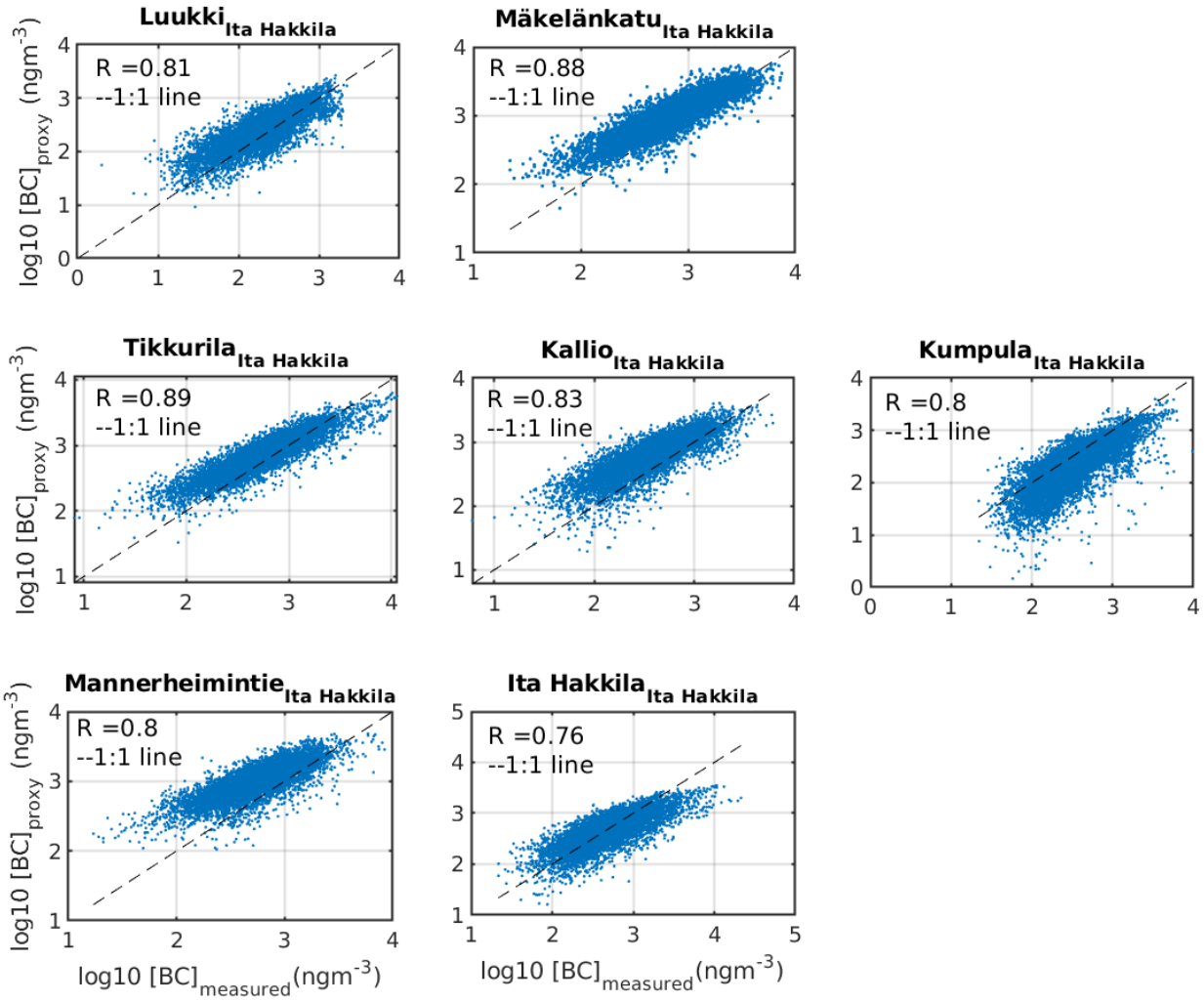

Supplementary figure 4: Proxy concentrations based on the Ita Hakkila proxy parameters often resulted in similar to the supplementary figure 3, where large variations in the placement of the 1:1 line is observed compared to the supplementary figure 2.

7. References

Aalto P., Hämeri K., Becker E., Weber R., Salm J., Mäkelä J.M., Hoell C., O'dowd C.D., Hansson H.-C., Väkevä M., Koponen I.K., Buzorius G., & Kulmala M., 2001. Physical characterization of aerosol particles duringnucleation events, Tellus B: Chemical and Physical Meteorology, 53:4, 344-358, DOI: 10.3402/tellusb.v53i4.17127.

Adachi, K., S. H. Chung, and P. R. Buseck , Shapes of soot aerosol particles and implications for their effects on climate, J. Geophys. Res., 2010 115, D15206, doi:10.1029/2009JD012868.

Alföldy, B.; Giechaskiel, B.; Hofmann, W.; Drossinos, Y. Size-distribution dependent lung deposition of diesel exhaust particles. J.Aerosol Sci. 2009, 40, 652−663.

Arnold F., Pirjola L., Aufmhoff H., Schuck T., .Lähde T., Hämeri K. First gaseous sulfuric acid measurements in automobile exhaust:Implications for volatile nanoparticle formation Atmospheric Environment 40, 2006, 7097–7105F.

Arnold F., Pirjola L., Rönkkö T., Reichl U., Schlager H., Lähde T., Heikkilä J. and Keskinen J., First online measurement of sulfuric acid gas in modern heavy-duty diesel engine exhaust: implications for nanoparticle formation. dx.doi.org/10.1021/es302432s, Environ. Sci. Technol. 2012, 46, 11227−11234.

Bond T.C., Streets D.G., Yarber K.F., Nelson S.M., Woo J-H., and Kilmont Z., A technology based global inventory of black and organic carbon emissions from combustion. JOURNAL OF GEOPHYSICAL RESEARCH, VOL. 109, D14203, 2004, doi:10.1029/2003JD003697.

Bond T.C. and Bergstrom R.W., Light absorption by carbonaceous particles: an investigative review. Aerosol Science and Technology, 40:27–67, 2006, DOI: 10.1080/02786820500421521.

Bond T. C., Zarzycki C., Flanner M. G., & Koch D. M., Quantifying immediate radiative forcing by black carbon and organic matter with the Specific Forcing Pulse, Atmos. Chem. Phys., 11, 1505–1525, 2011, doi:10.5194/acp-11-1505-2011.

Boucher, O., D. Randall, P. Artaxo, C. Bretherton, G. Feingold, P. Forster, V.-M. Kerminen, Y. Kondo, H. Liao, U. Lohmann, P. Rasch, S.K. Satheesh, S. Sherwood, B. Stevens and X.Y. Zhang, 2013: Clouds and Aerosols. In: Climate Change 2013: The Physical Science Basis. Contribution of Working Group I to the Fifth Assessment Report of the Intergovernmental Panel on Climate Change [Stocker, T.F., D. Qin, G.-K. Plattner, M. Tignor, S.K. Allen, J. Boschung, A. Nauels, Y. Xia, V. Bex

and P.M. Midgley (eds.)]. Cambridge University Press, Cambridge, United Kingdom and New York, NY, USA.

Brook R. D., Rajagopalan S., Pope III A., Brook J.R., Bhatnagar A., Diez-Roux A. V., Holguin F., Hong Y., Luepker R.V., Mittleman M.A., Peters A., Siscovick D., Smith S.C., Whitsel L., Kaufman J.D., Particulate matter air pollution and cardiovascular disease. 2004, American Heart Association, Inc. DOI: 10.1161/CIR.0b013e3181dbece1.

Carslaw K. S., Boucher O., Spracklen D.V., Mann G.W., Rae J.G.L., Woodward S., and Kulmala M. A review of natural aerosol interactions and feedbacks within the Earth system. 2010, Atmos. Chem. Phys., 10, 1701–1737.

Charlson R.J., Schwartz S.E., Hales J.M., Cess R.D., Coakley Jr J.A., Hansen J.E., Hofmann D.J., Climate forcing by anthropogenic aerosols. Science Volume 255, Issue 5043, 423-430, 1992.

Dada L., Paasonen P., Nieminen T., Mazon S.B., Kontkanen J. Peräkylä O., Lehtipalo K. Hussein T., Petäjä T., Kerminen V.-M., Bäck J., and Kulmala M., Long-term analysis of clear-sky new particle formation events and nonevents in Hyytiälä. Atmos. Chem. Phys., 17, 6227–6241, 2017. doi:10.5194/acp-17-6227-2017

Dal Maso M., Kulmala M., Lehtinen K.E.J., Mäkelä J.M., Aalto P., O,Dowd C.D. Condensation and coagulation sinks and formation of nucleation mode particles in coastal and boreal forest boundary layers. JOURNAL OF GEOPHYSICAL RESEARCH, VOL. 107, NO. D19, 8097, 10.1029/2001JD001053, 2002.

Dal Maso, M., Kulmala, M., Riipinen, I., Wagner, R., Hussein, T., Aalto, P. P. & Lehtinen, K. E. J., Formation and growth of fresh atmospheric aerosols: eight years of aerosol size distribution data from SMEAR II, Hyytiälä, Finland. 2005, Boreal Env. Res. 10: 323–336.

Donaldson K., Li X.Y. and MacNee W., Ultrafine (Nanometre) Particle mediated lung injury. J. Aerosol Sci. Vol. 29, No. 5/6, pp. 553—560, 1998.

Ehn M., Thronton J.A., Kleist E., Sipilä M., Junninen H., Pullinen I., Springer M., Rubach F., Tillmann R., Lee B. Lopez-Hilfiker F., Andres S., Acir I.-H., Rissanen M., Jokinen T., Schobesberger S. Kangasluoma J., Kontkanen J., Nieminen T., Kurten T., Nielsen L.B., Jorgensen S., Kjaergaard H.G., Canagaratna M., Dal Maso M., Berndt T., Petäjä T., Wehner A., Kerminen V.-M., Kulmala M., Worsnop D. R., Wildt J., & Mentel T.F. A large source of low-volatility secondary organic aerosol. Nature 506 476-479 2014. doi:10.1038/nature13032.

Enroth J., Saarikoski S., Niemi J., Kousa A., Jezek I., Mocnik G., Carbone S., Kuuluvainen H., Rönkkö., Hillamo R., and Pirjola L., Chemical and physical chareacterization of traffic particles in four different highway environments in the Helsinki metropolitan area. Atmos. Chem. Phys., 16, 5497–5512, 2016, doi:10.5194/acp-16-5497-2016.

Ferin J., Oberdörster G., and Penney D.P. Pulmonary retention of Ultrafine and fine particles in rats. Am. J. Respir. Cell Mol. Biol. Vol. 6. pp. 535-542, 1992.

Flanner M. G., Zender C. S., Hess P. G.,. Mahowald N. M, Painter T. H., Ramanathan V., and Rasch P. J. Springtime warming and reduced snow cover from carbonaceous particles, Atmos. Chem. Phys., 9, 2481–2497, 2009. www.atmos-chem-phys.net/9/2481/2009/

FMI news release, https://en.ilmatieteenlaitos.fi/press-release/539036550

Giechaskiel, B., Ntziachristos, L., Samaras, Z., Scheer, V., Casati, R., Vogt, R. Formation potential of vehicle exhaust nucleation mode particles on-road and in the laboratory. 2005. Atmospheric Environment 39 (2005) 3191–3198, doi:10.1016/j.atmosenv.2005.02.019.

Giechaskiel, B., Ntziachristos, L., Samaras, Z., Casati, R., Scheer, V., Vogt, R., 2007. Effect of speed and speed-transition on the formation of nucleation mode particles from a light duty diesel vehicle. SAE Tech. Paper Series, 2007-01-1110.

Giechaskiel, B.; Alföldy, B.; Drossinos, Y. A metric for health effects studies of diesel exhaust particles. J. Aerosol Sci. 2009, 40, 639−651.

Glassman I. And Yetter R. A. Combustion 4th ed. Amsterdam : Academic Press. 2008.

Hamed A., Minikin A., Harrison R.M., Talbot R., and Sun J. Explaining global surface aerosol number concentrations in terms of primary emissions and particle formation. Atmos. Chem. Phys., 10, 4775–4793, 2010. doi:10.5194/acp-10-4775-2010.

Hamed A., Korhonen H., Sihto S.-L., Joutsensaari J., Järvinen H., Petäjä T., Arnold F., Nieminen T., Kulmala M., Smith J.N., Lehtinen K.E.J., and Laaksonen A., The role of relative humidity in continental new particle formation. JOURNAL OF GEOPHYSICAL RESEARCH, VOL. 116, D03202, doi:10.1029/2010JD014186, 2011.

Hienola A. I., Pietikainen J.-P., Jacob D., Pozdun R., Petäjä T., Hyvarinen A.-P., Sogacheva L., Kerminen V.-M., Kulmala M., & Laaksonen A. Black carbon concentration and deposition estimations in Finlandby the regional aerosol–climate model, REMO-HAM, Atmos. Chem. Phys., 13, 4033–4055, 2013, doi:10.5194/acp-13-4033-2013.

Hussein T., Puustinen A., Aalto P.P., Mäkelä J.M., Hämeri K. and Kulmala M., Urban aerosol number size distribution. Atmos. Chem. Phys., 4, 391–411, 2004.

Hussein T., Martikainen J., Junninen H., Sogacheva L., Wagner R., Dal Maso M., Riipinen I., Aalto P., Kulmala M., Observation of regional new particle formation in the urban atmosphere. 2008 Tellus (2008), 60B, 509–521, DOI: 10.1111/j.1600-0889.2008.00365.x

Hussein T., Molgaard B., Hannuniemi H., Martikainen J., Järvi L., Wagner T., Ripamonti G., Weber S., Vesala T., and Hämeri K., Fingerprints of the urban particle number size distribution in Helsinki, Finland: Local versus regional characteristics. Boreal Env. Res. 19: 1–20, 2014.

Hussein T., Saleh S. S. A., Dos Santos V.N., Boor B.E., Koivisto A.J., and Londahl J., Regional inhaled deposited dose of urban aerosols in an eastern Mediterranean city. Atmosphere 2019,10, 530; doi:10.3390/atmos10090530

Hämeri, K., M. Väkevä, P. Aalto, M. Kulmala, E. Swietlicki, W. Seidl, E. Becker, and C. O'Dowd, Hygroscopic and CCN properties of aerosol particles in boreal forests, Tellus, Ser. B, 53, 359 – 379, 2001.

Jamriska M., Morawska L., & Mergersen K., The effect of temperature and humidity on size segregated traffic exhaust particle emissions, Atmospheric Environment 42 (2008) 2369–2382, doi:10.1016/j.atmosenv.2007.12.038.

Johnson, T. V. Diesel emission control in review. SAE International Journal of Fuels and Lubricants 1, 68–81 (2008).

Järvi L., Hannuniemi H., Hussein T., Junninen H., Aalto P.P., Hillamo R., Mäkelä T., Keronen P., Siivola E., Vesala T., Kulmala M. 2009: The urban measurement station SMEAR III: Continuous monitoring of air pollution and surface–atmosphere interactions in Helsinki, Finland. Boreal Environment Research 14 (suppl. A): 86–109.

Junninen H., Ehn M., Petäjä T., Luosujärvi L., Kotiaho T., Kostiainen R., Rohner U., Gonin M., Fuhrer K., Kulmala M., and Worsnop D.R. A high-resolution mass spectrometer to measure atmospheric ion composition. Atmos. Meas. Tech., 3, 1039–1053, 2010. doi:10.5194/amt-3-1039-2010.

Kittleson D. B. Engines and Nanoparticles: A review. J. Aerosol Sci. Vol. 29, No. 5/6, pp. 575—588, 1998

Kittelson, D. B.; Watts, W. F.; Johnson, J. P. On-road and laboratory evaluation of combustion aerosols-Part1: Summary of diesel engine results. J. Aerosol Sci. 2006, 37, 913-930.

Karjalainen, P., Rönkkö , T., Pirjola, L., Heikkilä , J., Happonen, M., Arnold, F., Rothe, D., Bielaczyc, P., Keskinen, J., 2014. Role of storage and release of sulphur compounds in diesel exhaust nucleation mode particle formation. Environ. Sci. Technol. 48, 2336 – 2343.

Karjalainen P., Timonen H., Saukko E., Kuuluvainen H., Saarikoski S., Aakko-Saksa P., Murtonen T., Bloss M., Dal Maso M., Simonen P., Ahlberg E., Svenningsson B., Brune W.H., Hillamo R., Keskinen J., & Rönkkö T., Time-resolved characterization of primary particle emissions andsecondary particle formation from a modern gasoline passenger car. Atmos. Chem. Phys., 16, 8559–8570, 2016. doi:10.5194/acp-16-8559-2016

Karpechko, A. Y., Charlton-Perez, A., Balmaseda, M., Tyrrell, N., & Vitart, F. (2018). Predicting sudden stratospheric warming 2018 and its climate impacts with a multimodel ensemble. Geophysical Research Letters, 45, 13,538–13,546. https://doi.org/10.1029/2018GL081091

Kontkanen J., Paasonen P., Aalto J., Bäck J., Rantala P., Petäjä T. & Kulmala M., Simple proxies for estimating the concentrations of monoterpenes and their oxidation products at a boreal forest site ' Atmospheric Chemistry and Physics 2016, vol. 16 , no. 20 , pp. 13291-13307. doi.org/10.5194/acp-16-13291-2016

Krecl P., Targino A. C., Landi T.P., and Ketzel M., Determination of black carbon, $PM_{2.5}$, particle number and NO_x emission factors from roadside measurements and their implications for emission inventory development. Atmospheric Environment 186, 229–240, 2018. doi.org/10.1016/j.atmosenv.2018.05.042.

Kurtenbach R., Kleffmann J., Niedojadlo A., & Wiesen P., Primary NO 2 emissions and their impact on air quality in traffic environments in Germany, 2012, Environmental Sciences Europe 2012, 24:21.

Kulmala M., Vehkamäki H., Petäjä T., Dal Maso M. , Lauri A., Kerminen V.-M. , Birmili W., McMurry P.H., Formation and growth rates of ultrafine atmospheric particles: a review of observations. Aerosol Science 35, 2004, 143 – 176, doi:10.1016/j.jaerosci.2003.10.003.

Kulmala M., Kontkanen J., Junninen H., Lehtipalo K., Manninen H.E., Nieminen T., Petäjä T., Sipilä M., Schobesberger S., Rantala P., Franchin A., Jokinen T., Järvinen E., Äijälä M., Kangasluoma J., Hakala J., Aalto P.P., Paasonen P., Mikkilä J., Vanhanen J., Aalto J., Hakola H.,

Makkonen U., Ruuskanen T., Mauldin R.L., Duplissy J., Vehkamäki H., Bäck J., Kortelainen A., Riipinen I., Kurtén T., Johnston M. V., Smith J.N., Ehn M., Mentel T.F., Lehtinen K.E.J., Laaksonen A., Kerminen V.M., Worsnop D.R., 2013. Direct observations of atmospheric aerosol nucleation. Science (80). 339, 943–946. https://doi.org/10.1126/science.1227385

Kuuluvainen H., Rönkkö T., Järvinen A., Saari S., Karjalainen P., Lähde T., Pirjola L., Niemi J.V., Hillamo R., and Keskinen J., Lung deposited surface area size distributions of particulate matter in different urban environment. Atmospheric Environment 136, 2016, 105 – 113, dx.doi.org/10.1016/j.atmosenv.2016.04.019.

Kuula J., Kuuluvainen H., Rönkkö T., V. Niemi J., Saukko E., Portin H., Aurela M., Saarikoski S., Rostedt A., Hillamo R., Timonen H., Applicability of Optical and Diffusion Charging-Based Particulate Matter Sensors to Urban Air Quality Measurements 2019. Accepted manuscript.

Künzi L. Krapf M., Daher N, Dommen J, Jeannet N, Schneider S, Platt S., Slowik J.G., Baumlin N., Salathe M., Prévôt A. S. H., Kalberer M., Strähl C., Dümbgen L., Sioutas C., Baltensperger U. & Geiser M. Toxicity of aged gasoline exhaust particles to normal and diseased airway epithelia. 2015 Nature scientific reports, 5:11801, DOi: 10.1038/srep11801.

Laakso L., Petäjä T., Lehtinen K.E.J., Kulmala M., Paatero J., Horrak U., Tammet H., & Joutsensaari J., Ion production rate in a boreal forest based on ion, particle andradiation measurements, 2004 Atmos. Chem. Phys., 4, 1933–1943.

Lenner M., Nitrogen dioxide in exhaust emissions from motor vehicles. Atmospheric Environment Vol. 21 No. 1, pp. 37-43, 1987.

Lehtinen K.E.J., Korhonen H., Dal Maso M. and Kulmala M., On the concept of condensation sink diameter. Boreal Env. Res. 8: 405–411. ISSN 1239-6095.

Lu Y., Yan C., Fu Y., Chen Y., Liu Y., Yang G., Wang Y., Bianchi F., Chu B., Zhou Y., Yin R,, Baalbaki R., Garmash O., Deng C., Wang W., Liu Y., Petäjä T., Kerminen V.-M., Jiang J., Kulmala M., & Wang L. A proxy for atmospheric daytime gaseous sulfuric acid concentration in urban Beijing. Atmos. Chem. Phys., 19, 1971–1983, 2019, https://doi.org/10.5194/acp-19-1971-2019

Lähde T., Rönkkö T., Virtanen A., Schuck T., Pirjola L. Hämeri K., Kulmala M., Arnold F., Tothe D., Keskinen J., Heavy duty diesel engine exhaust aerosol particle and ion measurement. Environ. dx.doi.org/10.1021/es801690h Sci. Technol. 2009, 43, 163–168.

Mahowald Natalie, Aerosol indirect effect on biogeochemical cycles and climate. 2011. doi: 10.1126/science.1207374.

Makkonen R., Asmi A., Kerminen V.M., Boy M., Arneth A., Hari P. and Kulmala M. Air pollution control and decreasing new particle formation lead to strong climate warming. Atmos. Chem. Phys., 12, 1515–1524, 2012. doi:10.5194/acp-12-1515-2012.

Metzger A., Verheggen B., Dommen J., Duplissy J., Prevot A.S.H., Weingartner E., Riipinen I., Kulmala M., Spracklen D.V., Carslaw K.S., Baltensperger U., Evidence for the role of organics in aerosol particle formation under atmospheric condition. PNAS, vol.107, no. 15, 2010, 6646-6651.

Meyer M.B., Patashnick H., L. Ambs J.& Rupprecht E. Development of a Sample Equilibration System for the TEOM Continuous PM Monitor, 2000, Journal of the Air & Waste Management Association, 50:8, 1345-1349, DOI:10.1080/10473289.2000.10464180

Mikkonen S., Romakkaniemi S. , Smith J.N., Korhonen H., Petäjä T., Plass-Duelmer C. , Boy M., McMurry P.H., Lehtinen K.E.J., Joutsensaari J., Hamed A., Mauldin III R.L. , Birmili W., Spindler G., Arnold F., Kulmala M., and Laaksonen A. A statistical proxy for sufuric acid concentration. Atmos. Chem. Phys., 11, 11319–11334, 2011. doi:10.5194/acp-11-11319-2011.

Nieminen, T., Asmi, A., Dal maso, M., P. Aalto, P., Keronen, P., Petäjä, T., Kulmala, M. & Kerminen, V.-M. 2014: Trends in atmospheric new-particle formation: 16 years of observations in a boreal-forest environment. Boreal Env. Res. 19 (suppl. B): 191–214.

Oberdörster G. Oberdörster E., Oberdörster J., Nanotoxicology: an emerging discipline evolving from studies of Ultrafine particles. Environmental health perspectives Volume 113, Number 7, 2005.

O'Dowd C.D., Jimenez J.L., Bahreini R., Flagan R.C., Seinfeld J.H., Hameri K., Pirjola L., Kulmala M., Jennings S.G. Hoffmann T., Marine aerosol formation from biogenic iodine emissions. Nature. 2002; 417(6889):632 636. doi:10.1038/nature00775.

Paasonen, P., Sihto, S.-L., Nieminen, T., Vuollekoski, H., Riipinen, I., Plaß-Dülmer, C., Berresheim, H., Birmili, W. & Kulmala, M.: Connection between new particle formation and sulphuric acid at Hohen-peissenberg (Germany) including the infl uence of organic compounds. Boreal Env. Res. 14: 616–629, 2009.

Paasonen P., Nieminen T., Asmi E., Manninen H.E., Petäjä T., Plass-Dülmer C., Flentje H., Birmili W., Wiedensohler A., Hõrrak U., Metzger A., Hamed A., Laaksonen A., Facchini M.C., Kerminen

V.-M., and Kulmala M. On the roles of sulfuric acid and low-volatility organic vapours in the initial steps of atmospheric new particle formation. doi:10.5194/acp-10-11223-2010. Atmos. Chem. Phys., 10, 11223–11242, 2010.

Paasonen P., Asmi A., Petäjä T., Kajos M. K., Äijälä M., Junninen H., Holst T., Abbatt J.P.D., Arneth A., Birmili W., Van der Gon H.D., Hamed A., Hoffer A., Laakso L., Laaksonen A., Leaitch W.R., Plass-Dulmer C., Pryor S.C., Räisänen P., Swietlicki E., Wiedensohler A., Worsnop D.R., Kerminen V.M. and Kulmala M. Warming-induced increase in aerosol number concentration likely to moderate climate change. 2013 DOI: 10.1038/NGEO1800, NATURE GEOSCIENCE VOL 6.

Paasonen P., Peltola M., Kontkanen J., Junninen H., Kerminen V.-M., & Kulmala M. Comprehensive analysis of particle growth rates from nucleationmode to cloud condensation nuclei in boreal forest, 2018 Atmos. Chem. Phys., 18, 12085–12103, https://doi.org/10.5194/acp-18-12085-2018.

Perez L., Medina-Ramon M., Kunzli N., Alastuey A., Pey J., Perez N., Garcia R., Tobias A., Querol X., Sunyer J. Size Fractionate Particulate Matter, Vehicle Traffic, and Case-Specific Daily Mortality in Barcelona, Spain VOL. 43, NO. 13, 2009 / ENVIRONMENTAL SCIENCE & TECHNOLOGY DOI: 10.1021/es8031488.

Petzold A., Schloesser H., Sheridan P., Arnott W.P., Ogren J.A. Virkkula A., Evaluation of multiangle absorption photometry for measuring aerosol light absorption. Aerosol Science and Technology, 39:40–51, 2005, DOI: 10.1080/027868290901945.

Petäjä T., Mauldin, III R.L., Kosciuch E., McGrath J., Nieminen T., Paasonen P., Boy M., Adamov A., Kotiaho T., and Kulmala M., Sulfuric acid and OH concentrations in a boreal forest site. Atmos. Chem. Phys., 9, 7435–7448, 2009.

Petäjä, T., Paasonen, P., Luoma, K., Vainio, T., Järvi, L., Kangasluoma, J., Niemi, J.V., Kousa, A., Portin, H., Timonen, H., Hatakka, J., Nousiainen, T., Harri, A.-M. and Kulmala, M. HAQT deliverable 4-1: Evaluation of current Kumpula AQ observations and benefits from two close-by supersites in Kumpula and in Mäkelänkatu, 2018.

Peräkylä O., Vogt M., Tikkanen O.-P., Laurila T., Kajos M. K., Rantala P. A., Patokoski J., Aalto J., Yli-Juuti T., Ehn M., Sipilä M., Paasonen P., Rissanen M., Nieminen T., Taipale R., Keronen P., Lappalainen H. K., Ruuskanen T. M., Rinne J., Kerminen V.-M., Monoterpenes' oxidation capacity and rate over a boreal forest: temporal variation and connection to growth of newly formed particles. Boreal Environment Research . 2014 Supplement B, Vol. 19, p293-310.

Pirjola L., Kulmala M., Wilck M., Bischoff A., Stratmann F., and Otto E., Formation of sulfuric acid aerosols and cloud condensation nuclei: an expression for significant nucleation and model comparison. J. Aerosol Sci. Vol. 30, No. 8, pp. 1079}1094, 1999.

Pirjola L., Paasonen P., Pfeiffer D., Hussein T., Hämeri K., Koskentalo T., Virtanen A., Römkkö T., Keskinen J., Pakkanen T.A., Hillamo R.E., Dispersion of particles and trace gases nearby a city highway: mobile laboratory measurements in Finland. Atmospheric Environment 40, 2006, 867–879, doi:10.1016/j.atmosenv.2005.10.018.

Pirjola L., Lähde T., Niemi J.V., Kousa A., Rönkkö T., Karjalainen P., Keskinen J., Frey A., Hillamo R., Spatial and temporal characterization of traffic emissions in urban microenvironments with a mobile laboratory, Atmospheric Environment 63, 2012, 156 – 167. http://dx.doi.org/10.1016/j.atmosenv.2012.09.022.

Platt S.M., El Haddad I., Pieber S.M., Zardini A.A., Suarez-Bertoa R., Clairotte M., Daellenbach K.R., Huang R.-J., Slowik J.G., Hellebust S., Temime-Roussel B., Marchand N., de Gouw J., Jimenez J.L., Hayes P.L., Robinson A.L., Baltensperger U., Astorga C. & Prévôt A.S.H. Gasoline cars produce more carbonaceous particulate matter than modern filter-equipped diesel cars. Scientific Reports, 7: 4926 , DOI:10.1038/s41598-017-03714-9, 2017.

Reche C., Viana M., Brines M., Perez N., Beddows D., Alastuey A., Querol X., Determinants of aerosol lung-deposited surface area variation in an urban environment. Science of the Total Environment 517, 2015, 38–47, dx.doi.org/10.1016/j.scitotenv.2015.02.049.

Ripamonti G., Järvi L., Molgaard B., Hussein T., Nordbo A., and Hämeri K., The effect of local sources on aerosol particle number size distribution, concentrations and fluxes in Helsinki, Finland. Tellus B 2013, 65, 19786, http://dx.doi.org/10.3402/tellusb.v65i0.19786.

Rohrer F. and Berresheim H. Strong correlation between levels of tropospheric hydroxyl radicals and solar ultraviolet radiation, Vol 442 2006 doi:10.1038/nature04924

Rönkkö T., Virtanen A., Vaaraslahti K., Keskinen J., Pirjola L., Lappi M., Effect of dilution conditions and driving parameters on nucleation mode particles in diesel exhaust: Laboratory and on-road study. doi:10.1016/j.atmosenv.2006.01.002, Atmospheric Environment 40 (2006) 2893–2901.

Rönkkö T., Virtanen A., Kannosto J. Keskinen J., Lappi M., Pirjola L., Nucleation mode particles with a nonvolatile core in the exhaust of a heavy duty diesel vehicle. ENVIRONMENTAL SCIENCE & TECHNOLOGY / VOL. 41, NO. 18, 2007 DOI: 10.1021/es0705339.

Rönkkö T., Lähde T., Heikkilä J., Pirjola L., Bauschke U., Aarnold F., Schlager H., Rothe D., Yli-Ojanperä J., Keskinen J., Effects of gaseous sulfuric acid on diesel exhaust nanoparticle formation and charecteristics. dx.doi.org/10.1021/es402354y, Environ. Sci. Technol. 2013, 47, 11882−11889.

Rönkkö T., Pirjola L., Ntziachristos L., Heikkilä J., Karjalainen P., Hillamo R., and Keskinen J., Vehicle engines produce exhaust nanoparticles even when not fueled. Environ. Sci. Technol. 2014, 48, 2043−2050. dx.doi.org/10.1021/es405687m.

Rönkkö T., Kuuluvainen H., Karjalainen P., Keskinen J., Hillamo R., Niemi J., Pirjola L., Timonen H.J., Saarikoski S., Saukko E., Järvinen A., Silvennoinen H., Rostedt A., Olin M., Yli-ojanperä J., Nousiainen P., Kousa A., Dal Maso M., Traffic is a major source of atmospheric nanocluster aerosol. PNAS , 2017 vol. 114 no. 29 7549–7554, www.pnas.org/cgi/doi/10.1073/pnas.1700830114.

Saarnio K., Niemi J.V., Saarikoski S., Aurela M., Timonen H., Teinilä K., Myllynen M., Frey A., Lamberg H., Jokiniemi J. and Hillamo R. (2012) Using monosaccharide anhy-drides to estimate the impact of wood combustion on fine particles in the Helsinki Metro-politan Area. Boreal Environ. Res.17, 163–183.

Seinfeld J.H. & Pandis S.N., Atmospheric Chemistry and Physics: From Air Pollution to Climate Change, 3rd Edition, 2016 ISBN: 978-1-118-94740-1

Shi J. P.; Harrison R. M. Investigation of ultrafine particle formation during diesel exhaust dilution. Environ. Sci. Technol. 1999, 33 , 3730-3736.

Spracklen D.V., Carslaw K.S., Merikanto J., Mann G.w., Reddington C.L., Pickering S., Ogren J.A., Andrews E., Baltensperger U., Weingartner E., Boy M., Kulmala M., Laakso L., Lihavainen H., Kivekäs N., Komppula M., Mihalopoulos M., Kouvarakis G., Jennings S.G., O'Dowd C., Birmili W., Wiedensohler A., Weller R., Gras J., Laj P., Sellegri K., Bonn B., Krejci R., Laaksonen A.,

Stockwell W.R. and Calvert J.G. The mechanism of the HO-SO_2 reaction, Atmospheric Environment Vol. 17 No. 11. pp. 2231-2235, 1983.

Timonen H., Teinilä K., Aurela M., Reyes F., Vásquez Y., Bloss M., Oyola P., Hillamo R., Asmi E., & Saarikoski S., Sources and composition of particulate matter in boreal arctic environment next to an active mining area, 2018, Boreal Env. Res. 23: 105–125.

Weber R.J., Marti J.J. and McMurry P.H. Measurements of new particle formation and ultrafine particle growth rates at a clean continental site. JOURNAL OF GEOPHYSICAL RESEARCH, VOL. 102, NO. D4., pages 4375-4385, 1997.

White Paper Pegasor AQ Urban 2018.

Yao L., Garmash O., Bianchi B., Zheng J., Yan C., Kontkanen J., Junninen H., Buenrostro Mazon S., Ehn M., Paasonen P., Sipilä M., Wang M., Wang X., Xiao S., Chen H., Lu Y., Zhang B., Wang D., Fu Q., Geng F., Li L., Wang H., Qiao L., Yang X., Chen J., Kerminen V.-M., Petäjä T., Worsnop D.R., Kulmala M. and Wang L. Atmospheric new particle formation from sulfuric acid and amines in a Chinese megacity 2018, Science 361 (6399), 278-281. DOI: 10.1126/science.aao4839